A Model Study of the Buoyancy-Driven Circulation in the Gulf of Maine

DAVID A. BROOKS

Department of Oceanography, Texas A&M University, College Station, Texas

(Manuscript received 12 February 1993, in final form 24 March 1994)

ABSTRACT

A quasi-linear prognostic numerical model has been used to study the three-dimensional baroclinic circulation in the Gulf of Maine region, with a focus on the buoyancy-driven circulation in the inner basins and near the coast where the influence of relatively fresh water from rivers and the Scotian shelf is important. The model uses a horizontal grid with 6-km resolution and a terrain-following vertical coordinate with ten levels to represent the bathymetry and stratification. Several model experiments explore the influences of fluxes from the principal rivers, tidal mixing, and shelf water inflow, beginning with a case with no initial horizontal density gradients and ending with cases initialized by temperature and salinity data from cruises in June of 1982 and 1983, augmented by climatological data. With composite initialization, the model develops a circulation containing realistic elements, including an anticlockwise gyre in the interior of the gulf and a prominent southwestward coastal current. For the 1982 case, characterized by relatively low river runoff, outflow from the Penobscot River guides a branch of the eastern Maine coastal current offshore in a thermohaline front 10–20 km east of Penobscot Bay; a similar dislocation is associated with the Kennebec and Androscoggin Rivers farther to the west. For the comparatively wet spring of 1983, the coastal current continues with less interruption from the Bay of Fundy to Cape Cod and consequently contributes less to the development of the interior circulation.

1. Background and introduction

The Gulf of Maine is defined on its landward side by an indentation of the North American coast and on its seaward side by several submarine banks (Fig. 1). Including the adjoining Bay of Fundy, the Gulf of Maine region extends about 600 km in the alongshore direction and about 400 km from the coast to the edge of the continental shelf. The shoal offshore banks restrict exchange between gulf water and warmer and more saline water from the Atlantic continental slope. The slope water enters the gulf as a seasonal deep inflow in the Northeast Channel, which transects the banks and provides the principal connection between the gulf and the Atlantic Ocean. Inside the gulf are three principal basins separated at the 200-m depth but connected by sills. Jordan and Wilkinson Basins have maximum depths of about 275 m, but Georges Basin, which forms the inner terminus of the Northeast Channel, contains the greatest interior depth at 380 m.

Because of its shape, the gulf–bay system experiences a nearly resonant co-oscillation with the semidiurnal (M_2) Atlantic tide (Garrett 1972). Spring tidal ranges exceed 15 m at the head of the Bay of Fundy and tidal currents of 1 m s^{-1} or larger occur over the offshore banks and the western Scotian shelf. The tidal current is rotary, with clockwise ellipses in the eastern gulf and over the banks and anticlockwise ellipses in the western gulf, where magnitudes generally decrease to 10–20 cm s^{-1} (Brown 1984). Tidal mixing overcomes stratification and maintains nearly uniform temperature and salinity over the shoal cap of Georges and Browns Banks, on the western shelf of Nova Scotia, and in parts of the Bay of Fundy (Loder and Greenberg 1986).

The nontidal circulation in the interior Gulf of Maine is basically an anticlockwise upper-level gyre that is distorted by bottom topography and influenced by surface heating and cooling, runoff from rivers, and inflowing waters from the Atlantic continental shelf and slope. The pioneering work by Bigelow (1927) showed that the interior gyre meshes on its offshore side with a seasonally closed clockwise flow around Georges Bank (Butman et al. 1982). The interior circulation intensifies in the spring and early summer months as stratification increases and weakens in the winter when intense surface cooling and convection erase much of the density structure in the upper water column (Bumpus and Lauzier 1965). In the winter, vertical overturning occurs at least to mid-depths in the basins (Brown and Beardsley 1978). Except in the eastern gulf and over the banks, where tidal mixing prevails year round, summer restratification near the surface seals off a mid-depth layer known as Maine intermediate water (MIW), whose distinguishing signature is a prominent temperature minimum (Hopkins and Garfield 1979). The MIW flows eastward along the northern edge of Georges Bank and is prominently exported from the gulf through the Northeast Channel.

Corresponding author address: Prof. David A. Brooks, Department of Oceanography, Texas A&M University, College Station, TX 77843.

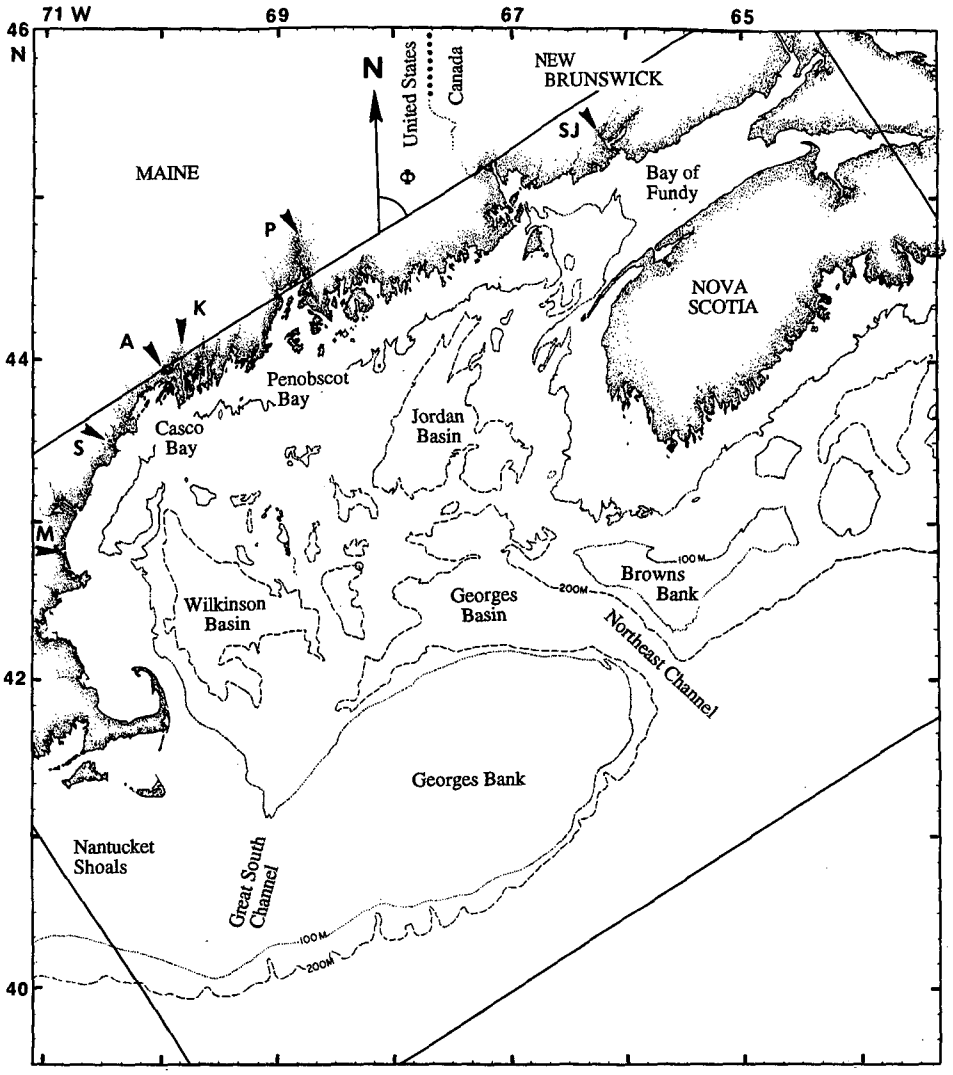

FIG. 1. Map of the Gulf of Maine region showing the principal basins and the offshore banks. Depth contours given for 100 (dotted) and 200 m (dashed). The major river entering the gulf is the Saint John (SJ); other principal rivers are the Penobscot (P), Kennebec (K), Androscoggin (A), Saco (S), and Merrimack (M). Mean river fluxes are given in Table 1. The inset box, rotated 58° from north, shows the intersection of the figure with the domain of the numerical model.

The baroclinic circulation in the gulf intensifies in the spring and early summer, when the seasonal contrast between buoyant nearshore waters and dense Atlantic slope water is most evident. Inflow of relatively fresh surface water from the Scotian shelf, influenced by river runoff into the Gulf of St. Lawrence, reaches a maximum in February (Smith 1989), whereas the maximum runoff from rivers inside the gulf occurs in April or May. Atlantic slope water, which is warm but relatively dense by virtue of its high salinity, enters the gulf as an episodic deep inflow in the Northeast Channel, with a minimum inward transport in the spring and a rapid increase to a maximum in early summer (Ramp et al. 1985). Inside the gulf, the dense slope water spreads over sills and pools in the bottom of the interior basins, where it contributes to the development of partially separated upper-level cyclonic gyres in Georges and Jordan Basins (Brooks 1985). A general southwestward flow is found in Wilkinson Basin (Vermersch and Beardsley 1979). In years with unusually large spring runoff, the slope water indraft may be delayed (Hopkins and Garfield 1979) and the Jordan Basin gyre may be weakened or even reversed (Brown and Irish 1992). The onset of upwelling-favorable summer southwesterly winds encourages the inward spreading of slope water over sills connecting the basins (Brooks 1987). Thus, in the summer months the interior waters of the central and western gulf have a three-layer structure: a thin layer of warm and fresh surface water overlies a somewhat saltier but much

colder and thicker layer of MIW, beneath which is found, in all seasons, the warmer but very salty and dense Maine bottom water, which derives much of its nature from the Atlantic slope.

The spring freshet from rivers entering the gulf produces an extensive band of low salinity nearshore water. Under the influence of the earth's rotation, the resulting buoyancy anomaly induces a southwestward upper-level coastal current revealed by drifter studies, sailing experience, and satellite imagery, as well as by hydrographic data and direct measurement of currents (Fig. 2). Of the six major rivers flowing into the gulf (Fig. 1), the Saint John River in New Brunswick delivers about one-third of the total mean freshwater flux (Apollonio 1979). The eastern Maine coastal current, which carries part of the low salinity plume from the Saint John River, in part turns offshore east of Penobscot Bay and in some years contributes to an anticlockwise surface gyre in the Jordan Basin that is evident in surface drifter tracks (Bigelow 1927) and in hydrographic and current measurements (Brooks 1985). The coastal current also delivers important fluxes of nutrients and phytoplankton to the central and western gulf (Brooks and Townsend 1989).

Modeling. Numerical simulations realistically reproduce the barotropic tide in the Bay of Fundy and the Gulf of Maine (Greenberg 1979). The tide wave rounds the western end of Nova Scotia and moves into the Bay of Fundy compressed against the Scotian side, and then reflects from the head of the bay and spreads southwestward to fill the rest of the gulf (Brooks 1993). Nonlinear rectification of tidal currents contributes to the clockwise flow around Georges and Browns Banks (Greenberg 1983; Isaji and Spaulding 1984; Wright et al. 1986), as predicted theoretically by Loder (1980). In a modeling review, Greenberg (1990) noted that further development requires the inclusion of internal density fields and their boundary counterparts in three-dimensional baroclinic numerical studies.

Isaji et al. (1984) conducted diagnostic model experiments in which the flow fields adjust to invariant density distributions determined from historical temperature and salinity data. Using a grid resolution of 25 km, they computed independent responses to seasonal forcing by the density field, the offshore tide, surface wind, and the alongshore pressure gradient on the Atlantic continental margin, with results that are consistent on a broad scale with the observed circulation

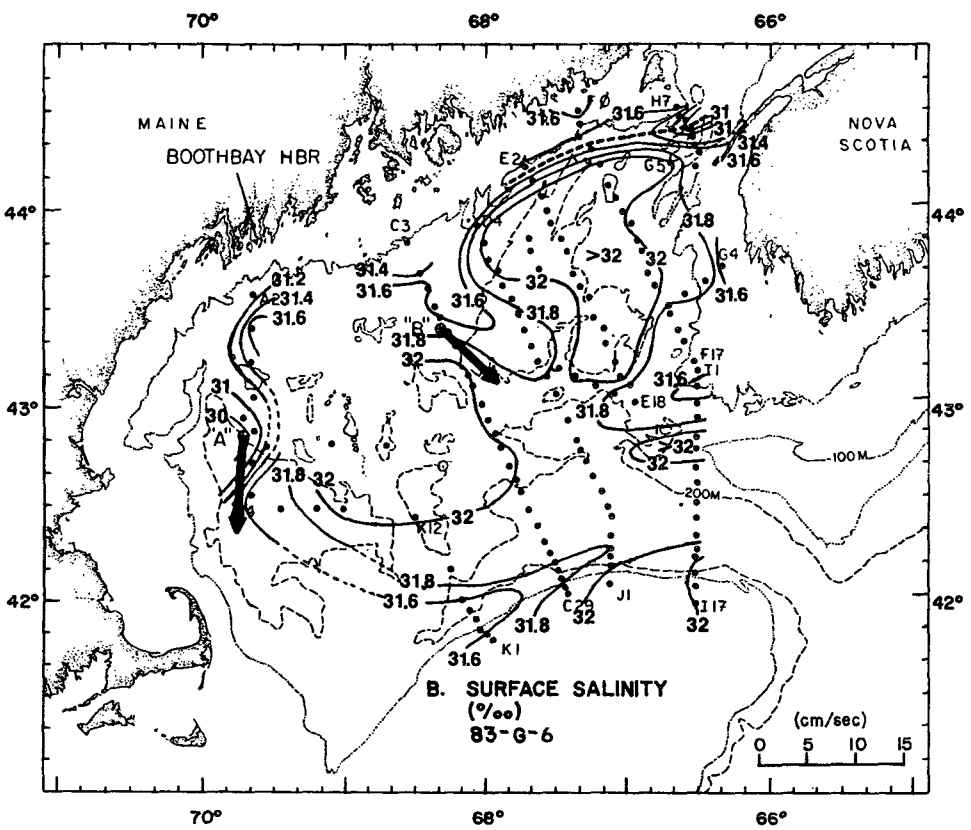

FIG. 2. Surface salinity in the Gulf of Maine from a survey conducted in June 1983 (from Brooks 1985). Hydrographic station locations are shown by the dots, and bottom contours are shown for 100 and 200 m. The heavy dashed curve traces an offshore salinity minimum from the mouth of the Bay of Fundy. Arrows show 10-week summer mean currents measured at depth 25 m (speed scale indicated).

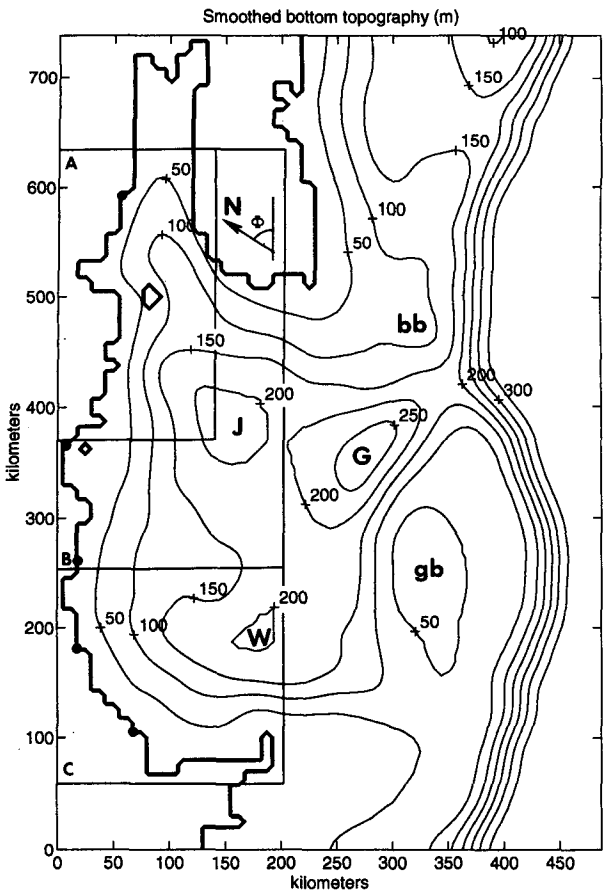

FIG. 3. Model representation of the Gulf of Maine region, showing smoothed bottom topography (contoured with 50-m interval) and the digitized coastal outline. An artificial bottom has been placed at 400 m on the seaward side of the continental shelf. The full model domain, rotated 58° clockwise from north, is shown relative to geographical coordinates in Fig. 1. The labeled basins inside the gulf are Jordan (J), Georges (G), and Wilkinson (W); the shoal regions offshore are Georges Bank (gb) and Browns Bank (bb). The inset rectangles identify model subdomains shown in later figures, as follows: inset A (Figs. 4, 5); inset B (Figs. 13, 14); and inset C (Figs. 15, 16). Dots placed on the coastal boundary indicate the mouths of the principal rivers identified in Fig. 1.

patterns in the gulf. More recently, Lynch et al. (1992) used a model with a refined grid to compute diagnostic responses to alongshelf wind stress, Scotian shelf inflow, and the summer baroclinic density structure near Georges Bank. Their results show realistic detail, including reasonable transports in the Northeast Channel, a weak eastern Maine coastal current, and a tidal front around Georges Bank with a mixed zone atop the bank.

The present paper describes results from experiments with a prognostic model in which the temperature and salinity fields (and thus the density) are coupled with and evolve with the flow fields. The study focuses on the influence of river runoff and the associated development of the coastal current and interior circulation in the gulf. After a brief description of the model, we begin by examining the influence of a single river (the Saint John) flowing into a stratified but initially resting model ocean that includes a smoothed representation of the bottom topography, the offshore banks, the continental shelf, and the coastal outline. In this configuration there is no potential energy available in the initial state and the only forcing is provided by the buoyancy injection from the river. The first experiment ignores the tides and is not realistic in its representation of the large-scale density structure of the gulf, but it is a natural extension of the numerical study by Chao and Boicourt (1986) who examined the consequences of freshwater from an estuary entering a flat-bottom continental shelf sea with a straight coastline and initially homogeneous background density. The bulk of the paper is concerned with the second experiment, which includes the influences of all the major rivers, the semidiurnal tide, and the inflow from the Scotian shelf.

2. Model description

The numerical model is called MECCA (Model for Estuarine and Coastal Circulation Assessment: Hess 1989; Johnson and Hess 1990). The appendix gives a summary of the model equations, the boundary conditions, and the implementation method. In the present application, the model is forced at its open boundaries by tides, mean sea level height, and thermohaline fields, and at its coastal boundary by freshwater fluxes from rivers. The effects of the wind and seasonal heating are not considered at this stage. The model fields were represented in the vertical on a sigma or terrain-following vertical coordinate with 10 equally spaced levels and in the horizontal on a rectangular 120 by 80 grid with uniform resolution of 6.25 km. The model bottom topography was interpolated from a digital database with horizontal resolution of about 8 km and then smoothed with a three-by-three point bilinear filter (Fig. 3) to reduce pressure gradient errors over steep bottom slopes (Haney 1991). In deep water offshore of the continental slope, a false bottom of 400 m was used to limit the external time step.

The numerical scheme uses parameterized turbulence to represent vertical and horizontal eddy viscosity and diffusion. Vertical mixing is parameterized with a mixing length and Richardson number dependence, and horizontal mixing is a function of local velocity shear and the grid spacing, as explained in the appendix. For the present application, the linearized momentum equations are solved for the velocity and coupled conservation equations are solved for temperature and salinity, which are linked to the density field by an empirical equation of state. Except for the turbulence parameterization, the MECCA formalism is very similar to that given by Blumberg and Mellor (1987).

3. Experiment one: Initially "flat" stratification

Chao and Boicourt (1986, herein CB) investigated the case of estuarine outflow into a shelf sea with a flat bottom and a straight coastline. They used a numerical model with five levels in the vertical to study the development of the baroclinic flow field over a several week period. In their experiments, a freshened bulge or bolus forms near the estuary mouth. Within the bulge the flow generally turns anticyclonically. After about 10 days, a small but intense cyclonic transition region develops near the bulge boundary, and a low salinity extrusion "leaks" out of the cyclone to form a right-bounded coastal plume that propagates away from the source region in the Kelvin wave sense. With moderate values of vertical mixing, they found that the coastal plume expands as an upper-level current without a counterflowing undercurrent, whereas inside the bulge the circulation is more complex, with undercurrent structures and downwelling in regions of cyclonic flow. With increased vertical mixing, they found that a secondary cyclonic region develops near the center of the expanding boundary of the freshened bulge, ultimately producing a two-cell flow pattern that partially divides the bulge. In all of their experiments the coastal plume escapes the bulge in a sharp transition region marked by downwelling and strong cyclonic turning of the surface currents.

Taking the results of CB as a starting point, we first examine the response of the present model to outflow from the Saint John River, without considering other forcing factors such as tides or winds, but including variable bottom depth and an irregular coastal outline. The volume flux from the river was set at 3×10^3 $m^3 s^{-1}$, or about three times the 30-year annual mean (Apollonio 1979). The river flux was held constant for 30 days to approximate a spring freshet. The gulf water into which the river flows was initialized with vertical temperature and salinity profiles typical of spring conditions near the mouth of the Bay of Fundy but without initial horizontal gradients; that is, for the first experiment there was no potential energy available in the background state, and the model response develops solely as a result of advection and diffusion of the buoyancy anomaly derived from the river flux. In the model cell containing the river mouth, the salinity and temperature were held constant at 5 ppt and 9°C at all levels, so the experiment advances from an initial state that includes the full thermohaline influence of the river near its mouth.

In later experiments that included the energetic tidal currents of the Gulf of Maine, it was necessary to drop the advection terms from the momentum equations to maintain numerical stability (see appendix). For consistency, the linearized momentum equations were also used in the tide-free experiments, although several fully nonlinear cases have been explored with weaker or absent tides. In all experiments discussed here the advection terms were retained in the conservation equations for temperature and salinity, which gives a quasi-linear, 3D prognostic scheme that retains the self-advective character of the buoyancy-driven flow.

In their experiments, CB investigated cases with constant vertical mixing coefficients in the range 1–5 ($\times 10^{-4}$ $m^2 s^{-1}$). In the present model, the vertical mixing and diffusion coefficients depend on vertical shear and density stratification through a Richardson number and mixing length parameterization as explained in the appendix, and thus a direct comparison against CB's simpler scheme is not possible. However, as a first test of the present model, a value of 1×10^{-4} $m^2 s^{-1}$ is chosen for the background vertical mixing coefficient (A_0) to parallel CB's "low friction" case. The resulting formation of the freshened bulge and the expansion of the coastal plume are illustrated in Figs. 4 a–c, which show the surface salinity and velocity fields near the mouth of the Bay of Fundy at 10, 20, and 30 days after the start of the experiment. The fields are shown only for the subdomain of the inset box labeled A in Fig. 3, but the full model domain was used for the experiment. Salinities in the range 30–31 psu are shaded to highlight the expanding frontal zone that separates the bulge and plume from the waters of the gulf. Schematic interpretations of the flow fields are shown in the corresponding panels of Fig. 5, in which the 31.5 psu contour (dashed curve) shows the approximate location of the plume boundary, and the speed of the surface current is qualitatively indicated by the width of the hollow arrows.

As the freshened bulge expands outward from the river mouth, most of the contained surface water turns anticyclonically in the cum sole direction of the coastal Kelvin wave. However, part of the bulge boundary also spreads in the opposite direction, and the surface water defining that part of the bulge first turns cyclonically before joining the anticyclonic movement (region "a" in Fig. 5) along the bulge boundary toward the Maine coast. At 10 days the coastal plume is just beginning to separate from or "leak" out of the bulge in a region of developing cyclonic circulation labeled "c" in Fig. 5a, which corresponds to the transition zone identified by CB in their Fig. 6. The plume spreads into Passamaquoddy Bay and moves toward the channel separating Grand Manan Island from the Maine coast (place names are identified in Fig. 5c). Subsequently, the cyclone c intensifies and the plume expands along the coast at about 5 km d^{-1}, leaving the bulge behind but extracting freshened water from it. By 20 days the coastal current has reached Frenchman Bay (Fig. 5b), and by 30 days it is approaching Blue Hill Bay with flow speeds of 10–15 cm s^{-1} in Grand Manan Channel (Fig. 5c); by day 45 (not shown) the leading edge of the plume has reached the eastern entrance to Penobscot Bay.

Since the frontal width scale of the baroclinic coastal plume is expected to be set by the Rossby radius (Gill

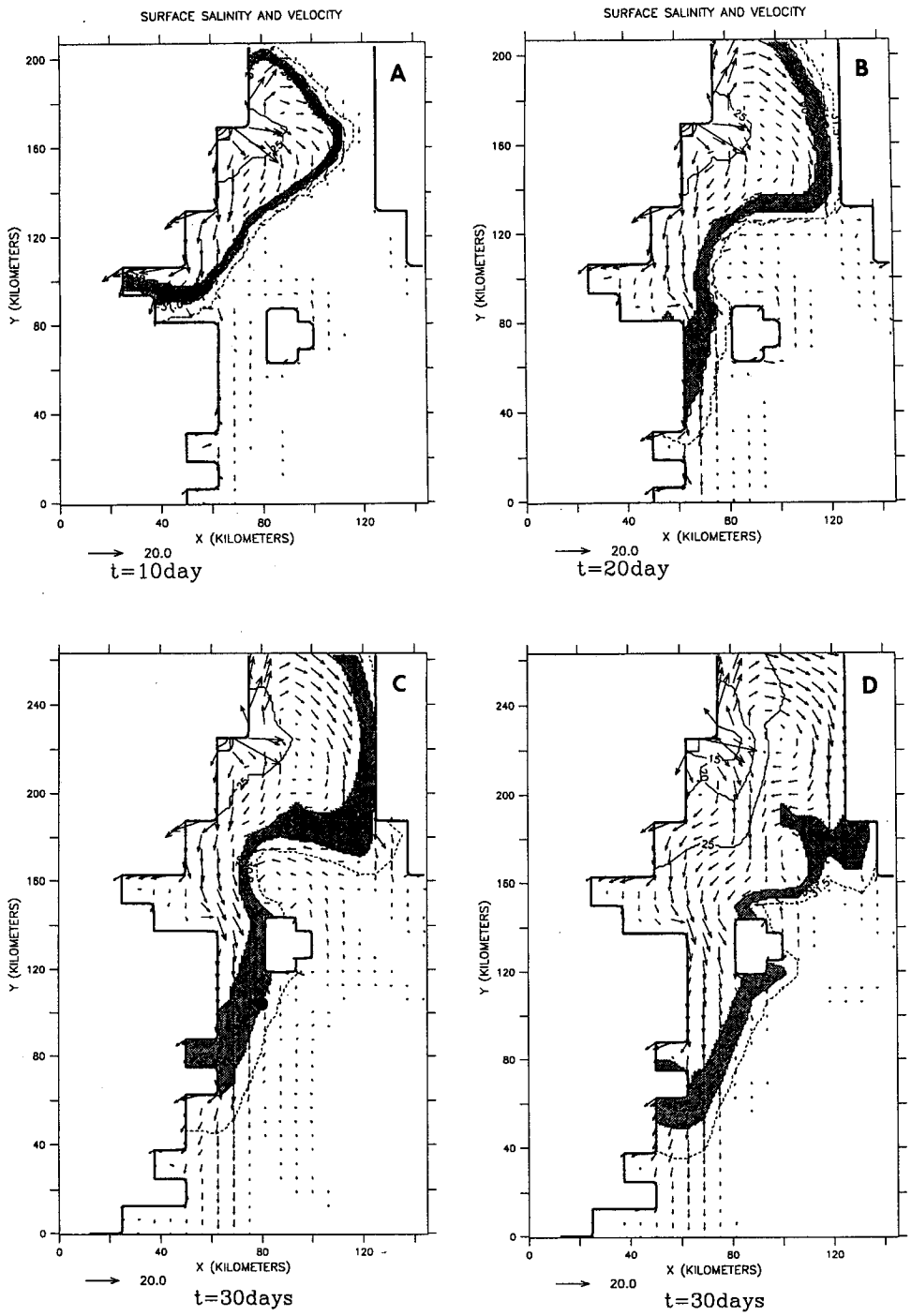

FIG. 4. Model surface velocity and salinity after 10, 20, and 30 days [panels (a), (b), and (c)], showing the development of the outflow from the Saint John River. The domain of the figure is shown by inset box A in Fig. 3. The river mouth is located at the hollow square. The velocity scale is shown by the horizontal arrow at the bottom of each panel. Salinity contours are shown for 10–30 ppt with interval 5 ppt (solid), and also for 31.5 ppt (dashed). The expanding boundary of the river plume is indicated by the shaded region, which includes salinities between 30 and 31 ppt. Panel (d) is the same as (c) except for increased vertical mixing (see text). The island is Grand Manan Island. The solid circle in panel (c) shows the location of a calculation referred to in text.

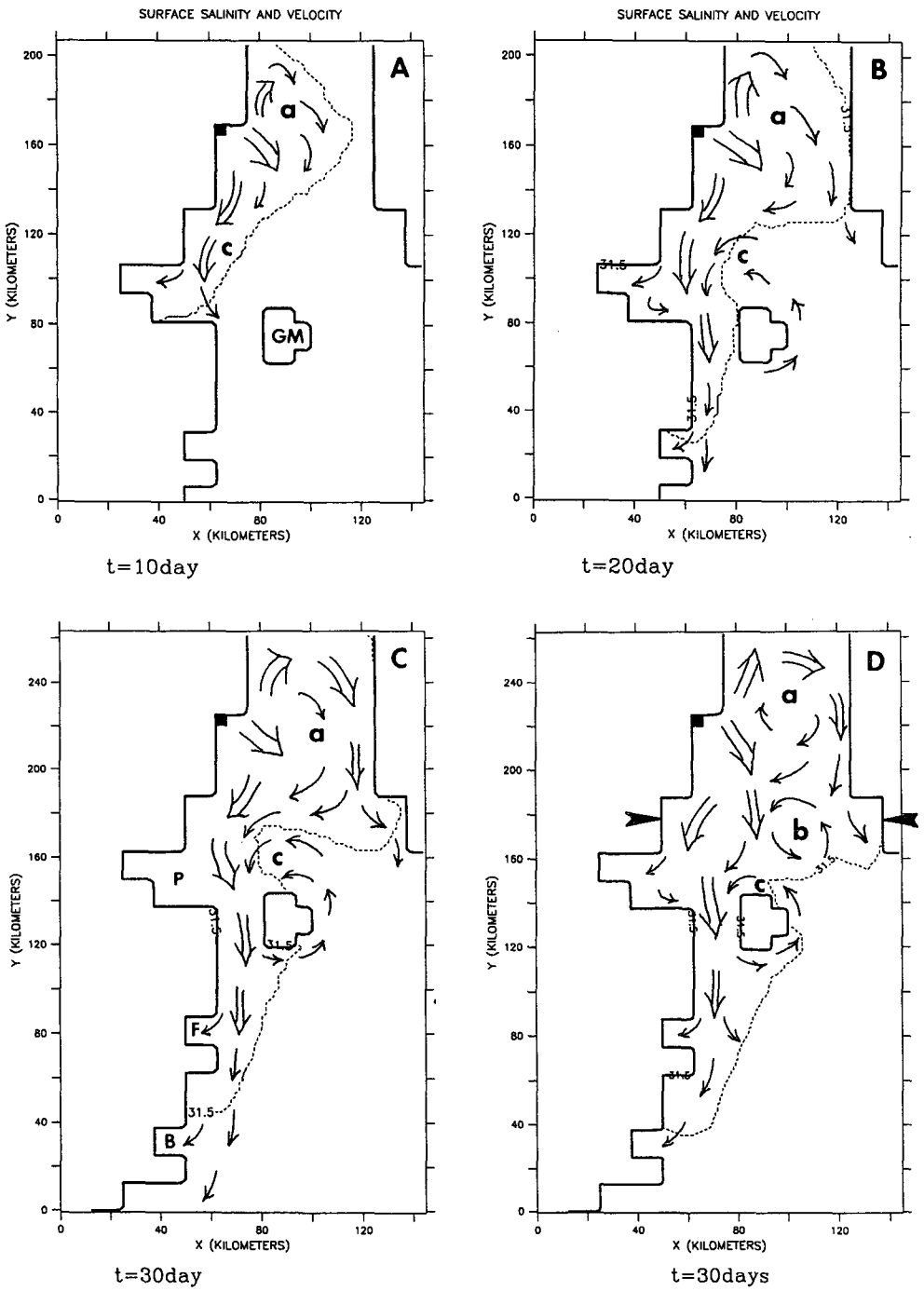

FIG. 5. Schematic interpretation of the surface flow fields shown in Fig. 4. The magnitude of the current is qualitatively indicated by the width of the double arrows. The 31.5 ppt salinity contour (dashed) is shown to indicate the edge of the expanding river plume. The river mouth location is shown by the solid square. The letters "a" and "c" indicate regions of anticyclonic and cyclonic development, respectively; the letter "b" identifies a second cyclonic eddy (d). Grand Manan Island (GM) is indicated in (a), and the coastal bays labeled in (c) are Passamaquoddy (P), Frenchman (F), and Blue Hill (B). The horizontal arrowheads on panel (d) mark the ends of a vertical section shown in Fig. 7.

1982), a model grid sufficiently fine to resolve dynamical adjustments on that scale is necessary. After 30 days, the maximum stability frequency (N) in a water column near the edge of the expanding coastal plume (solid circle in Fig. 4c) was 2.2×10^{-2} s^{-1}, determined by a pycnocline density difference of 1.2 sigma-t units

between depth levels 12 m and 36 m at that location. The associated first-mode Rossby radius, $R_D = NH/f$, where H is the local depth (109 m) and f is the Coriolis parameter (1.1×10^{-4} s^{-1}), is 21.8 km. Thus, the frontal scale spans three or four grid cells with spacing 6.25 km and the coastal plume should be reasonably resolved, at least near that location. However, to provide an independent check, the experiment just described was repeated with a halved grid scale of 3.13 km, giving a factor of 4 increase in the number of grid elements per modeled area. It was necessary to limit the refined grid to the northeastern quadrant of the original model domain, because halving the grid scale multiplies the required computing time by at least eight. The limited domain is useful in tide-free experiments but not in cases that must include the tides, because the full model domain with the continental shelf is required to reproduce the tidal resonance of the Gulf of Maine region. With the limited model domain the additional artificial boundaries become important in long integrations, but the essential elements of the river bulge and plume expansion shown in Figs. 4 and 5 are recovered. However, the evolution proceeds more slowly because the effective horizontal turbulent mixing is reduced by a factor of 4 when the grid scale is halved (see the appendix). Based on the refined-grid experiments, it is concluded that the development of the coastal plume is adequately resolved by the full model grid with 6.25-km horizontal spacing.

The development in Figs. 4 and 5 strongly resembles the first example shown by CB, particularly with regard to the intensification of a cyclonic root cell that forms a transition between the bulge and the expanding coastal plume. In the present case, the root cyclone strengthens and expands to encircle Grand Manan Island by day 30, redirecting the surface flow back toward the river mouth on the offshore side of the island. There are two principal surface freshwater paths: one adjacent to the Maine coast, and the other along the fringe of the bulge, near the western shore of Nova Scotia.

In June 1983 observations from the eastern Gulf of Maine revealed a path of low salinity surface water moving seaward between Grand Manan Island and the Nova Scotian shore (Fig. 2). The minimum salinity offshore of the island (<30.5 psu) was significantly lower than that found adjacent to the Maine coast (<31.6 psu). This indicates a direct path from the Saint John River mouth to the region offshore of the island, since there are no other major freshwater sources nearby and the minimum salinity is too low to be explained by water from the Scotian shelf (Smith 1983). The observed salinity along a vertical section from the "H line" crossing the mouth of the Bay of Fundy is shown in Fig. 6. The lowest surface value was found at station H-5, roughly midway between the Nova Scotian shore and Grand Manan Island. (Station locations are shown in Fig. 2.) The corresponding temperature section (Brooks and Gottlieb 1985) reveals that the

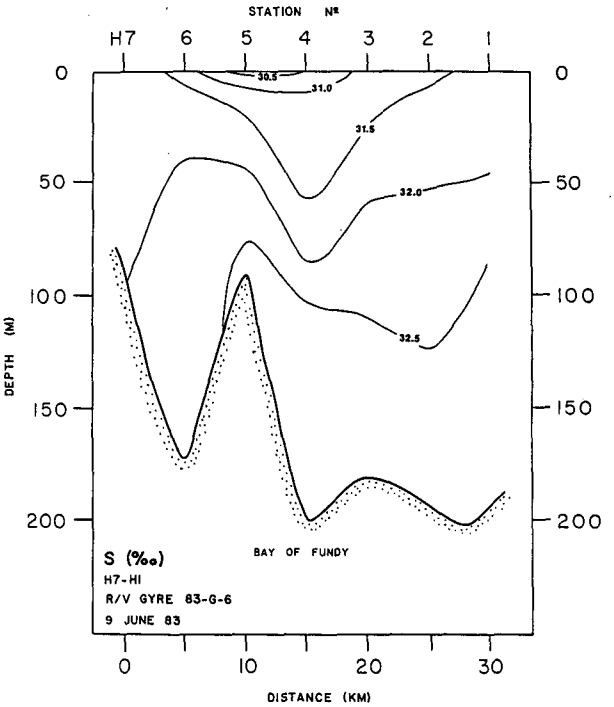

FIG. 6. Salinity (ppt) on a vertical section along the H transect between Grand Manan Island and Nova Scotia in June 1983; the view is inward toward the Bay of Fundy. The station locations are shown in Fig. 2. The offshore surface salinity minimum between stations 4 and 5 is associated with the Saint John River outflow, from Brooks and Gottlieb (1985).

salinity minimum was associated with a warm surface anomaly, which is consistent with the slightly warmer river water compared to the colder surrounding surface temperatures outside the freshwater pathway.

The spring of 1983 was characterized by heavy runoff and an unusually fresh nearshore band of coastal water, but an explanation for the even lower salinity found offshore of Grand Manan Island was not available at the time of the survey (Brooks 1985). The model results shown in Figs. 4 and 5 suggest that the anticyclonic circulation in the outer part of the expanding river bulge provides an offshore pathway for river-freshened surface water, whereas the nearshore branch of low salinity water is carried by the coastal current adjacent to the Maine coast.

Returning to the model studies, CB noted the formation of a two-cell pattern in the river bulge region when the vertical mixing was increased. To investigate the sensitivity of the present model to vertical mixing, an additional experiment was run with the background vertical mixing coefficient increased to 25×10^{-4} m^2 s^{-1}; otherwise, the second experiment was identical to the first. For comparison, the surface salinity and velocity fields at 30 days (only) are shown in Fig. 4d, and the corresponding schematic interpretation of the surface flow field is given in Fig. 5d.

With increased vertical mixing, a second region of cyclonic flow develops in the central part of the expanding fringe of the bulge, in accord with the findings of CB. The new feature begins as an anticlockwise "kink" in the fringe of the bulge and then grows to form a cyclonic eddy with a partially closed surface circulation, indicated as feature "b" in Fig. 5d. The new or secondary eddy circulation favors a direct path for the river outflow between Grand Manan Island and Nova Scotia at the expense of the longer path around the fringe of the bulge, which is partly short-circuited by the eddy. As in the low-friction case, the original or root cyclone c envelops Grand Manan Island and is associated with the freshened surface plume that moves southwestward along the Maine coast.

It was also noted by CB that the secondary cyclone divided the river bulge into two parts separated by a region of downwelling, and a similar result is found here. Figure 7 shows a model vertical section that slices through the river bulge, including the cyclonic eddy labeled "b" in Fig. 5d (the section ends are indicated by horizontal arrowheads). The flow in the downcoast direction (in the Kelvin wave sense adjacent to the Maine coast) is shown by the solid contours, and the superimposed vectors show the velocity in the plane of the figure. After 30 days, the freshwater branch that moves toward the offshore side of Grand Manan Island extends essentially to the bottom, whereas the inshore branch that feeds the coastal current has a more baroclinic structure with a countercurrent at depth. The return (inward) limb of cyclone b, shown by the region of dashed contours and negative velocities centered near 60 km on the abscissa, is also deep rooted but with a subsurface maximum at about 30-m depth. The velocity vectors in the plane of the figure show that the flow converges in the center of the cyclone. Downwelling occurs in the inward limb, where the surface flow turns cyclonically, and upwelling occurs between the outward limb and the nearshore countercurrent, in a region where the surface flow turns anticyclonically to avoid the island ahead. The maximum vertical speed is about 10^{-2} cm s^{-1}, corresponding to a vertical displacement of order 10 m d^{-1}. The mechanism of the plume evolution is not pursued here, but downwelling in regions of cyclonic flow is consistent with a simple vorticity balance in which the development of cyclonic eddies in the expanding fringe of the river bulge is accompanied by vertical stretching of fluid columns and deepening of the flow structure in the cyclones.

The model experiments described here employed a "slip" bottom boundary condition and 10 uniformly spaced sigma levels in the vertical, so the details of a logarithmic bottom boundary layer are not expected to be resolved. With much finer vertical resolution to represent the structure of near-bottom turbulent mixing, a no-slip bottom boundary condition could be used to allow the development of a log layer and the bottom stress vector τ_b could be calculated directly from the

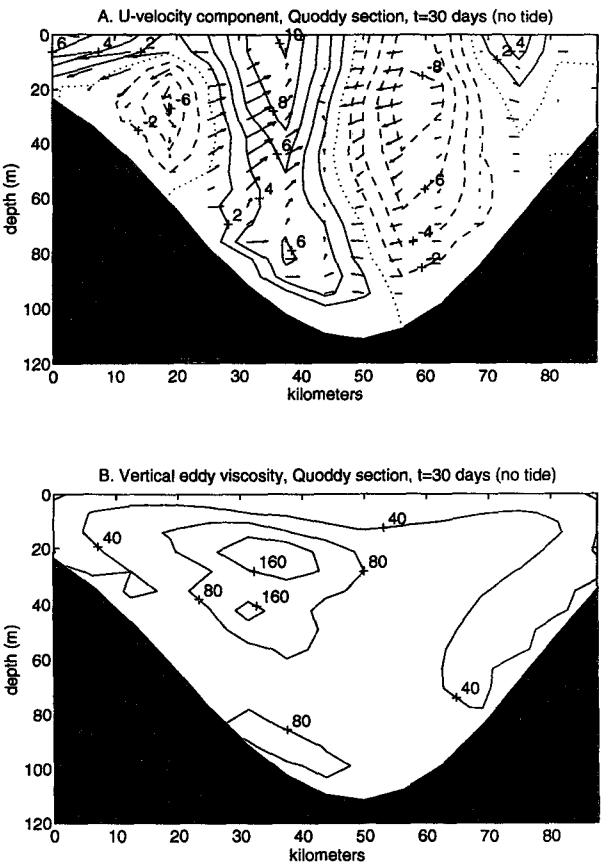

FIG. 7. Model vertical section crossing the river plume and cyclonic eddy b between Passamaquoddy Bay and Nova Scotia (see Fig. 5d for location); the view is inward toward the Bay of Fundy. The top panel shows the alongshore velocity component (cm s^{-1}) at t = 30 d; solid contours indicate southwestward flow along the coast in the Kelvin wave direction. The vectors show the velocity in the plane of the section. Vertical exaggeration is 1000. Lower panel shows effective vertical eddy viscosity (cm^2 s^{-1}), which depends on stratification and velocity shear as defined in the appendix. Successive contours indicate a doubling of the eddy viscosity.

velocity shear (Davies 1993). In such cases, the bottom boundary-layer thickness would be given by $\mathbf{u}^*/f$, where $\mathbf{u}^* = (\tau_b/\rho)^{1/2}$ is the friction velocity, or a more complicated formula could be used to estimate the bottom stress as a function of static stability (Weatherly and Martin 1978). In the present case, the bottom stress is calculated from a parameterized quadratic drag law and a stress-matching condition is applied at the bottom boundary, as described in the appendix. An estimate of the scale height of the bottom boundary layer is provided by the turbulent Ekman layer thickness $(A_V/f)^{1/2}$. Figure 7b shows contours of the effective vertical eddy viscosity A_V on the section through the river bulge and the cyclonic eddy b in Fig. 5. Successive contours indicate a doubling of A_V. At the time of the velocity section in Fig. 7a the vertical eddy viscosity increased from near its background value of 25×10^{-4}

$m^2 s^{-1}$ close to the surface, where the shear is small and the Richardson number large, to about 160×10^{-4} $m^2 s^{-1}$ at depth 20–40 m in the outward branch of cyclone b, where relatively large velocity shear reduces the Richardson number to small values. Approaching the bottom, A_V decreases to about 80×10^{-4} $m^2 s^{-1}$ near the greatest depth on the section (109 m). The indicated boundary-layer thickness is about 10 m, which at that depth is only marginally represented by two sigma levels in a 10-level scheme. On the edges of the section, particularly beneath the developing coastal river plume where the depth is about 30 m, A_V is about 40×10^{-4} $m^2 s^{-1}$ and the indicated boundary-layer thickness is about 6 m, which is resolved by three sigma levels. In the next experiments, which include the tides, near-bottom vertical mixing is stronger and the bottom boundary layer is better represented.

4. Evolution of the coastal current and interior circulation

Bigelow (1927) pointed out that inflowing water from the continental shelf of Nova Scotia plays an important role in the vernal intensification of the circulation in the Gulf of Maine. Based on current measurements on the Scotian shelf during 1979–80, Smith (1983) found a southwestward annual mean transport of 1.4×10^5 $m^3 s^{-1}$, most of which rounds the western end of Nova Scotia and enters the gulf. He noted a distinct annual signal in the transport, with a maximum inflow of about 5×10^5 $m^3 s^{-1}$ in late winter, when the water carries a low salinity anomaly from the previous spring's runoff into the Gulf of St. Lawrence; a minimum transport near zero occurred in the summer months. Based on analysis of hydrographic and oxygen isotope data, Chapman and Beardsley (1989) showed that part of the southwestward flow on the Scotian shelf, particularly over the shelf break, is a continuation of the larger-scale flow in the Labrador Basin, which joins with the Labrador Current and then follows the shelf edge to the south.

To simulate the influence of the Scotian shelf inflow in a barotropic model of the region, Wright et al. (1986) used an "upstream" boundary condition in which the sea level was exponentially set up 0.1 m against the Nova Scotian end of the open boundary crossing the shelf. They estimated that the appropriate cross-shelf trapping scale for the sea level setup was in the range 24–58 km, depending on the value of the bottom drag coefficient, the bottom slope, and the distance from the model boundary location to the end of the Scotian shelf at Cabot Strait. For their model geometry and with linear bottom friction, Wright et al. (1986) chose a trapping scale of 39 km. They noted that the setup was consistent with either a spatially uniform 0.1-Pa wind stress acting along the shelf toward the Gulf of Maine or with a southwestward barotropic transport of about 7×10^5 $m^3 s^{-1}$, comparable to the winter geostrophic transport across a Halifax section calculated by Drinkwater et al. (1979) and about the same as the maximum transport into the Gulf of Maine calculated by Smith (1983), based on measured currents. For the following model experiments, a similar exponential boundary condition was used to effect inflow from the Scotian shelf. The trapping scale was set at 58 km, reflecting differences in the geometry of the present model (primarily a longer shelf region). Numerous experiments were run with different trapping scales, and the results do not depend critically on the value chosen.

a. Initial data

In the first experiment the model was initialized with depth-dependent temperature and salinity fields without horizontal gradients, so the isopycnals were initially "flat." To more closely approximate the actual conditions during the vernal spinup phase of the circulation, the following experiments were initialized at all levels in each cell with temperature and salinity data from a high-resolution hydrographic cruise conducted in June 1982, augmented by June climatological data in regions of the model domain not visited by the cruise. Thus, the model integrates forward from an initial state with a distribution of available potential energy determined from springtime data. Spring 1982 was characterized by relatively low precipitation and river runoff, compared to 1983. The locations of the cruise stations and the climatological stations (from the Levitus dataset) are shown in Fig. 8, along with the surface salinity contoured from the combined dataset. The cruise stations were typically separated 10 km or less, and the Levitus dataset is gridded on a one-degree square. Bilinear interpolation and a three-point smoothing filter were used to set the initial values of temperature and salinity at each sigma level in each grid cell of the model; the initial sea level height was zero in all grid cells. The composite initial datasets provide maximum resolution in the inner gulf and coastal strip, which is the focal region for the present model study, while the much coarser Levitus dataset provides a convenient and climatologically consistent way to extend the initial data to the rest of the model domain.

The following experiments also included the influence of the six principal rivers that flow into the gulf. The locations of the river mouths are indicated in Figs. 1 and 3 (the Kennebec and Androscoggin Rivers are grouped as a single source because they have a common mouth at Merrymeeting Bay). Table 1 shows the annual mean river fluxes (Apollonio 1979). The temperatures in the grid cells containing the river mouths were set at the June values shown in Table 1, and the salinity was set at 5 ppt to account for initial mixing in the river cells. For the dry spring of 1982, the model river fluxes were set equal to the annual means.

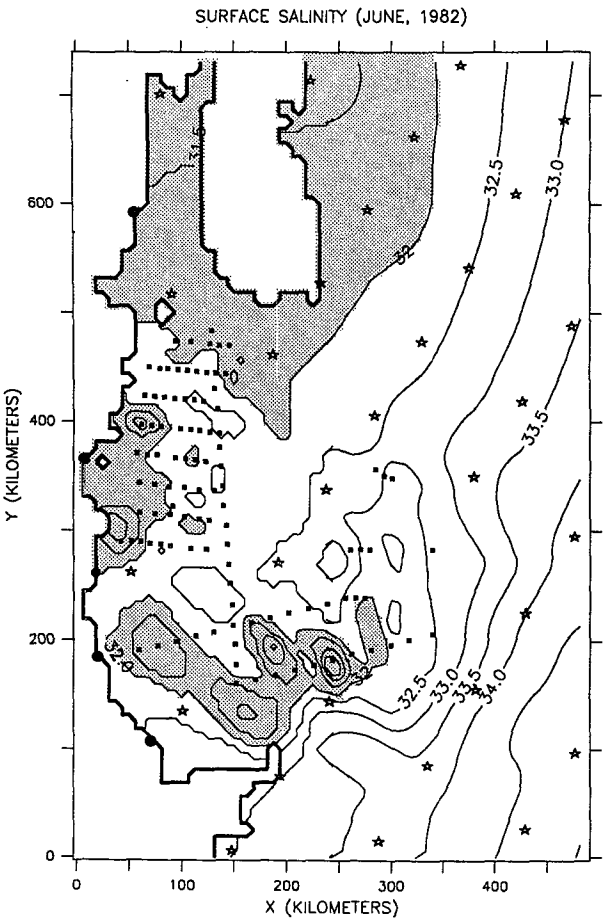

FIG. 8. Composite surface salinity (ppt) for the full model domain in Fig. 1 used to initialize a model experiment. The salinity data (and corresponding temperature data, not shown) are from a June 1982 hydrographic survey cruise (station locations shown by solid squares), augmented by June climatological data (available on a 1° grid at locations shown by the stars). Dots indicate the mouths of the major rivers, identified in Fig. 1. The contour interval is 0.5 ppt. The shaded area indicates surface salinities less than 32 ppt.

A full simulation of the circulation was not the present goal, so the river fluxes were held constant during the experiment. In future simulation experiments, more extensive initial datasets can be used, and the time history of the model river runoff can be tailored to approximate the actual conditions in a particular year.

b. Tides

Because of near-resonance, the semi-diurnal tides in the Gulf of Maine region are unusually energetic. Tidal stirring maintains relatively well-mixed waters over the shoal offshore banks and on the western Scotian Shelf, and the resulting frontal zones separating mixed regions from stratified ones play an important role in determining the baroclinic, non-tidal circulation (Loder and Greenberg 1986; Butman et al. 1982). Nonlinear rectification of barotropic tidal currents over steep bottom slopes also contributes to the nontidal flow by adding a circulation component in the clockwise sense around shoal banks and shelves (e.g. Loder and Wright 1985; Wright et al. 1986). It is important to note that the tidal-rectification component of the total circulation is absent in the present experiments because the nonlinear momentum terms have been excluded, as explained in the appendix. Numerical models have successfully reproduced the amplitude and phase of the principal lunar semidiurnal (M_2) sea level and current oscillations in the Gulf of Maine–Bay of Fundy region, both in vertically integrated and three-dimensional formulations (Greenberg 1979; Sucsy et al. 1993).

The focus of the present study is the low-frequency or tidal-residual component of the total circulation, particularly in the interior gulf and the coastal region where the influence of river buoyancy sources is likely to be most important and tidal rectification is less important. However, because of the significance of tidal mixing, it is necessary that the model be able to reproduce the dominant semidiurnal tidal response, and this requires that the model domain include the offshore banks and continental shelf to properly represent the tidal resonance. In the following experiments, tidal forcing was supplied at the ends of the open boundaries by varying the sea level height sinusoidally with the M_2 period (12.42 h). The forcing amplitude, taken from cotidal maps of the region was 0.5 m at the Scotian Shelf boundary and 0.4 m at the Cape Cod boundary. The only other forcing supplied for the cases discussed here was the exponential sea level setup against Nova Scotia, previously described; in particular, the important influences of surface wind stress and seasonal heating are not considered.

The character of the tidal response is shown by the model sea level height distribution during one-quarter of an M_2 period (Fig. 9) and by the surface velocity

TABLE 1. Annual mean volume fluxes and June water temperatures for the principal rivers entering the Gulf of Maine.

	River				
	Saint John	Penobscot	Kennebec–Androscoggin	Saco	Merrimack
Mean flux ($m^3 s^{-1}$)	1020	413	476	159	222
Temperature (°C)	9	10	11.5	12	12.5

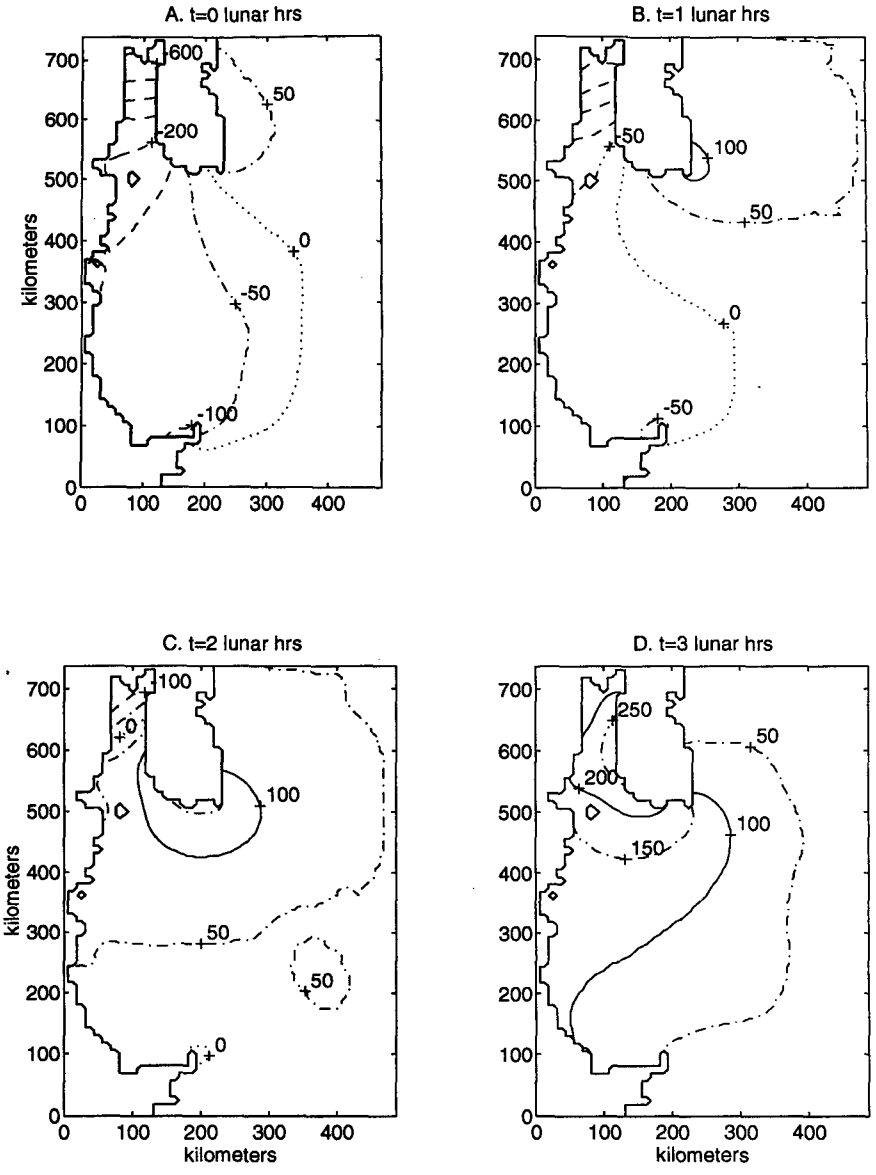

FIG. 9. Model sea level height (cm) during a quarter-cycle of the semidiurnal (M_2) tide, beginning at $t = 0$ lunar hours when sea level is near its low value at the upper end of the Bay of Fundy. The full model domain is shown. Dashed contours indicate negative values, with a contour interval of 100 cm; solid contours indicate positive values, with the same interval. Also shown are the zero (mean level) contour (dotted) and several intermediate contours at 50-cm interval (dash-dotted).

vectors at quadrature phases of the tidal currents (Fig. 10). The model time step was set at 62.1 s to exactly synchronize the 12.42 h M_2 tidal period and to allow calculation of the tidal-residual fields by averaging over one tidal cycle (720 model time steps). The sequence begins at lunar hour 0 when the sea level at the upper end of the Bay of Fundy is near its low value (less than 6 m, Fig. 9a) and the flood has just begun (Fig. 10a). The approaching tide wave moves southwestward along the outer Scotian shelf, and the sea level rises rapidly as the wave rounds the tip of Nova Scotia and enters the Bay of Fundy, confined against the Scotian side (Figs. 9b–d). The resonant amplification factor or gain between the Atlantic tide and that at the head of the Bay of Fundy is about 10. After 3 lunar hours, or one-quarter of the M_2 period (3.105 hs), the flood is near its maximum in the Bay of Fundy, where the surface currents exceed 2 m s^{-1} in the narrow entrances to the upper arms of the bay (Fig. 10b). Current speeds in excess of 1 m s^{-1} occur over the shoal cap of Georges

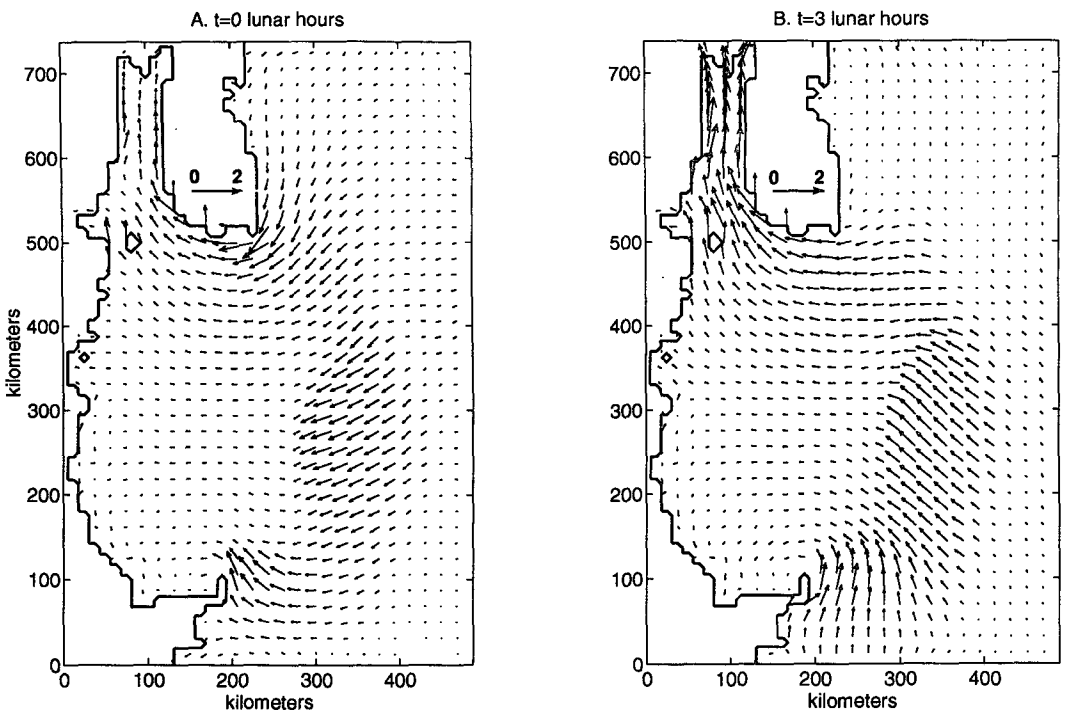

FIG. 10. Model surface velocity at quadrature phases of a semidiurnal cycle, corresponding to the sea level height at $t = 0$ and $t = 3$ lunar hours shown in Fig. 9. For clarity, the vector field has been decimated by a factor of 3; that is, only 1/9 of the total vector field is shown. The speed scale (m s^{-1}) is indicated.

Bank and also near Cape Cod and the tip of Nova Scotia. The surface currents are rotary with elliptical hodographs and clockwise vector rotation over Georges Bank and most of the interior gulf, except in the far western gulf where much weaker current vectors rotate anticlockwise. During the rest of the M_2 cycle (see Brooks 1993) the rising tide wave reflects from the head of the Bay of Fundy, rapidly filling it, and then spreads southwestward along the New England coast with diminished amplitude, so that upon reaching Boston the tidal range is reduced to about 3 m and the tidal currents are less than 0.5 m s^{-1}. The ebb first begins at about 4 lunar hours near the "elbow" of Cape Cod and near Cape Sable Island off the southeastern tip of Nova Scotia, while the flood continues over Georges Bank and into the Bay of Fundy. At about 6 lunar hours, when the current vectors over Georges Bank have rotated offshore, the ebb stage finally reaches the upper Bay of Fundy. The tidal features of the present model are generally in agreement with observations (Brown 1984) and also with other tidal models (Greenberg 1979; Sucsy et al. 1993).

c. *The large-scale response*

Figure 11 shows the tidal-residual sea level height for the full model domain at 10, 20, and 30 days after the June 1982 initialization, and also at 30 days after an otherwise identical experiment that was initialized with data from the "wet" June of 1983. Figure 12 shows the tidal-residual surface currents and surface temperature relative to the bottom topography after 30 days for both cases; for clarity, the velocity vectors have been decimated by two in each direction, so only one-fourth of the vectors appear. The tidal-residual fields were determined by averaging over one M_2 tidal period (720 model time steps of 62.1 s) at various times in the experiment.

Although the initial sea level height was zero everywhere, the structure evolves rapidly and the principal elements are established by day 10. Those elements are, for the 1982 case, relatively low sea level over the central basins of the gulf, an isolated high over the shoal cap of Georges Bank, and a shoreward rise that extends from the upstream boundary on the Scotian Shelf throughout the interior gulf to Cape Cod. At later times the freshened river plumes expand, nearshore sea level setup increases, and by day 30 the coastal current extends from the Saint John River to Cape Cod. Outside the river plumes, the range of sea level variation after 30 days in both 1982 and 1983 is about 7 cm, comparable to the range of sea surface dynamic height variation calculated from June 1983 hydrographic data (Brooks 1985).

The sea level setup on the upstream boundary drives a southwestward nearshore surface flow that mostly

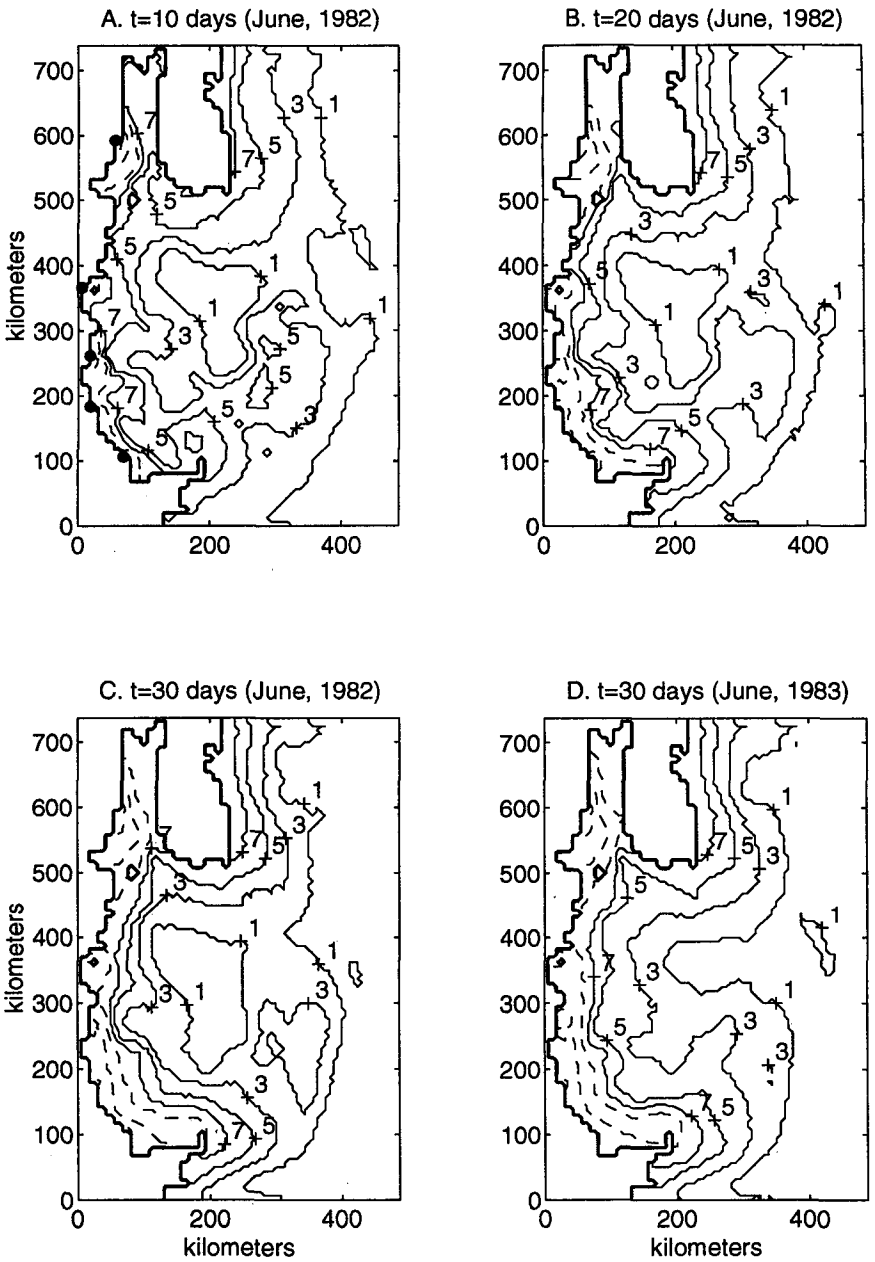

FIG. 11. Tidal-residual sea level height (cm) for the full model domain at (a) 10, (b) 20, and (c) 30 days in an experiment initialized with the composite dataset for June 1982. The residual fields are determined by averaging over one semidiurnal period. Panel (d) shows the result at 30 days for an analogous experiment initialized with composite data from June 1983, which was a spring characterized by high river runoff. Solid contours are shown with 2-cm interval. Dashed contours near the coast are shown for elevations of 10, 15, and 20 cm. The dots in (a) show the location of the mouths of the principal rivers identified in Fig. 1.

rounds the tip of the Scotian peninsula, where cold deep water is mixed up to the surface by energetic tidal currents. The inflow around Nova Scotia enters the Bay of Fundy and then partially retroflects to join the eastern Maine coastal current, which carries most of the Saint John River flux and is particularly strong between Grand Manan Island and Penobscot Bay. The retroflection at the mouth of the Bay of Fundy was noted by Bigelow (1927) in his schematic surface circulation, and the same tendency is clear in the trajectories of many drift bottles launched in spring months from the lightship *Lurcher* off the tip of Nova Scotia (Bumpus 1960).

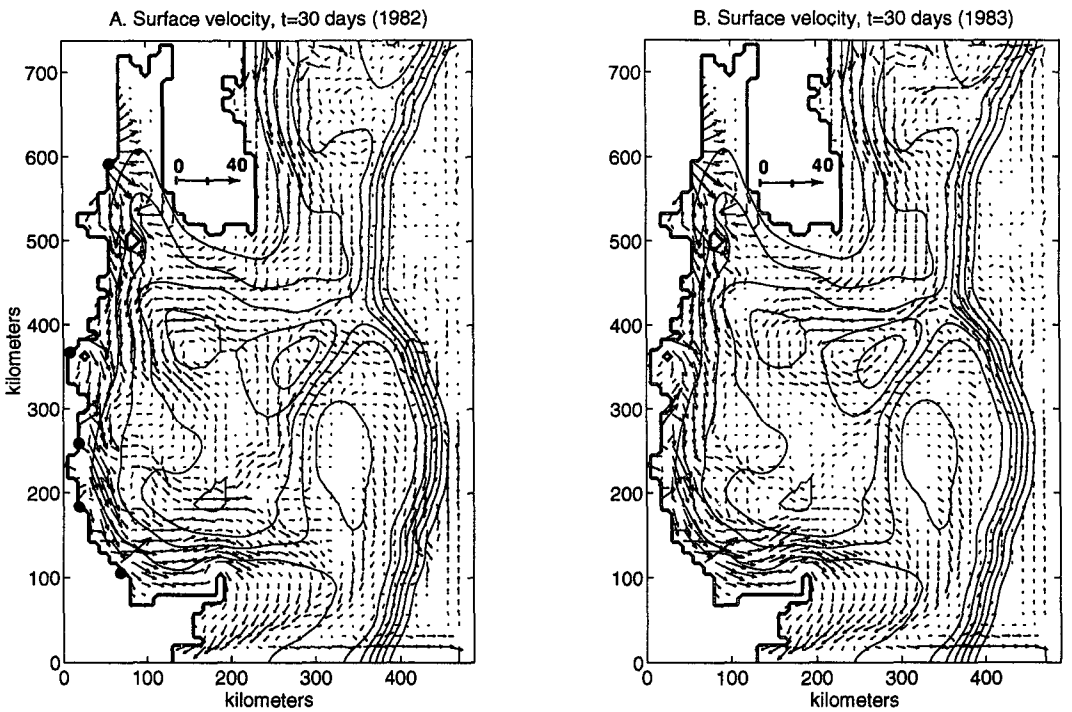

FIG. 12. Tidal-residual surface velocity for the full model domain at t = 30 days for experiments initialized with composite data from (a) June 1982 and (b) June 1983, including runoff from the principal rivers located by the dots. River fluxes for the 1982 case are given in Table 1. For the wet year of 1983 the fluxes were set at three times the values shown in Table 1. In both cases, flow into the gulf is forced by a steady exponential setup of the sea surface slope along the open boundary crossing the Scotian shelf (see text). The smoothed model bottom topography is shown by the solid contours (unlabeled; see Fig. 3). The vectors have been decimated by a factor of 2 for clarity; that is, only one-fourth of the vector field is shown. The speed scale (cm s^{-1}) is indicated.

The coastal current carries cold, low salinity surface water southwestward along the eastern Maine coast. Upon reaching Blue Hill Bay, near the eastern entrance to Penobscot Bay, the coastal current is partially deflected or guided offshore in the thermohaline front formed by the outflow from the Penobscot River. The deflection is more evident in 1982, when part of the offshore flow contributes to a general anticlockwise circulation in the gulf (Fig. 12). In the full-gulf model, the grid resolution is inadequate to represent the intricate coastal details and many islands in Penobscot Bay, but the separation of the coastal current appears to be influenced by the expanding freshwater bulge from the river as it moves seaward in the passages between the outer islands in the bay (principally Vinalhaven and Isleboro) and the headland immediately to the east. Nearshore surface salinity data from the Penobscot region show the freshest water leaving the western side of the bay, but a frontal zone with low salinities east of the outer bay islands is also evident (Graham 1970). The coastal current re-forms immediately west of Penobscot Bay but it is interrupted again by a similar front that forms to the east of the Kennebec–Androscoggin River mouth, and to a lesser extent by the smaller outflow from the Saco and Merrimack Rivers farther along the coast. In the southwestern gulf, the river water is a few degrees warmer than the ocean waters, so the plumes are evident as warm anomalies that bend along the coast toward Cape Cod, where most of the coastal current moves over Nantucket Shoals to the continental shelf offshore in general accord with hydrographic and drifter observations from the region (Limeburner and Beardsley 1982).

The separated portion of the eastern Maine coastal current contributes to a partially closed surface anticlockwise gyre in Jordan Basin and the western end of Georges Basin (Fig. 12). The anticlockwise circulation is better defined after 30 days in the 1983 experiment than in the 1982 case. In the western gulf, the coastal current continues toward Cape Cod and then exits to the shelf to the south. However, an interior branch separates from the coastal current where it is interrupted by the thermohaline front from the Kennebec–Androscoggin River plume. The interior branch crosses Wilkinson Basin toward Georges Bank, where it flows northeastward along the inner flank of the bank and then mostly back toward Jordan Basin, where some of the water rejoins the eastern Maine coastal current. The resulting large-scale anticlockwise circulation in the central gulf, more prominently developed in the

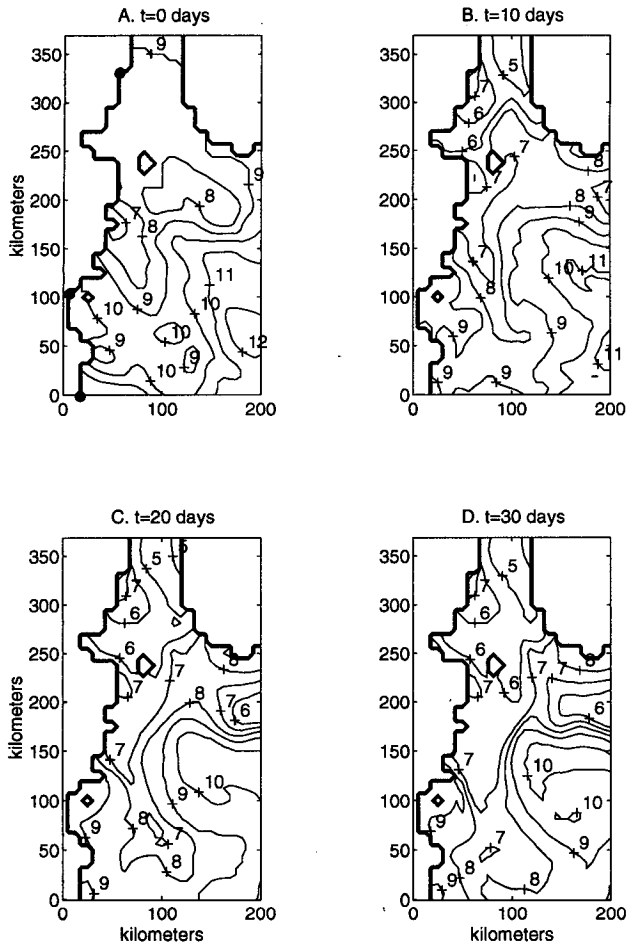

FIG. 13. Tidal-residual surface temperature (°C) for the model subdomain labeled B in Fig. 3, showing the development of the eastern Maine coastal current after 10, 20, and 30 days, starting from the June 1982 initial condition at $t = 0$ days. Contour interval is 1°C. River mouths indicated by the dots.

1982 experiment than in 1983, is appropriately called the Bigelow gyre. Part of the offshore limb of this gyre turns seaward around the eastern tip of Georges Bank, where it joins a southwestward flow along the shelf break. Tidal mixing maintains relatively cool surface temperatures over the eastern and western ends of the bank. There is little indication of clockwise recirculation around the shallow cap of Georges Bank, as is sometimes suggested by observations (Butman et al. 1982), but this may be explained by the absence of tidal rectification in the model experiments.

The background section of this paper shows that the evolving model surface circulation just described has some features in common with the upper-level water movements inside the gulf inferred by various investigators over many years. Some of the similarity is of course "built in," because the model was initialized with a dataset that contributed to the inferred circulation against which the model result is compared. However, the sea level was initially flat in the model experiments, and most of the initializing data were confined to the eastern half of the gulf, which excludes the offshore shelf region, most of Georges Bank, and the nearshore coastal strip where much of the influence of river runoff is confined. Thus, the similarity between the modeled and inferred patterns lends confidence in the model's ability to represent the evolving physical structures of the buoyancy-driven flow. We now examine the model results for the inner gulf in greater detail.

d. The coastal current

Figures 13 and 14 show the tidal-residual surface temperature and salinity fields from the northeastern portion of the gulf (inset "B" in Fig. 3) at the initial time and after 10, 20, and 30 days for the 1982 model experiment. The patchiness of the initial fields, particularly the salinity, reflects the limitations of the avail-

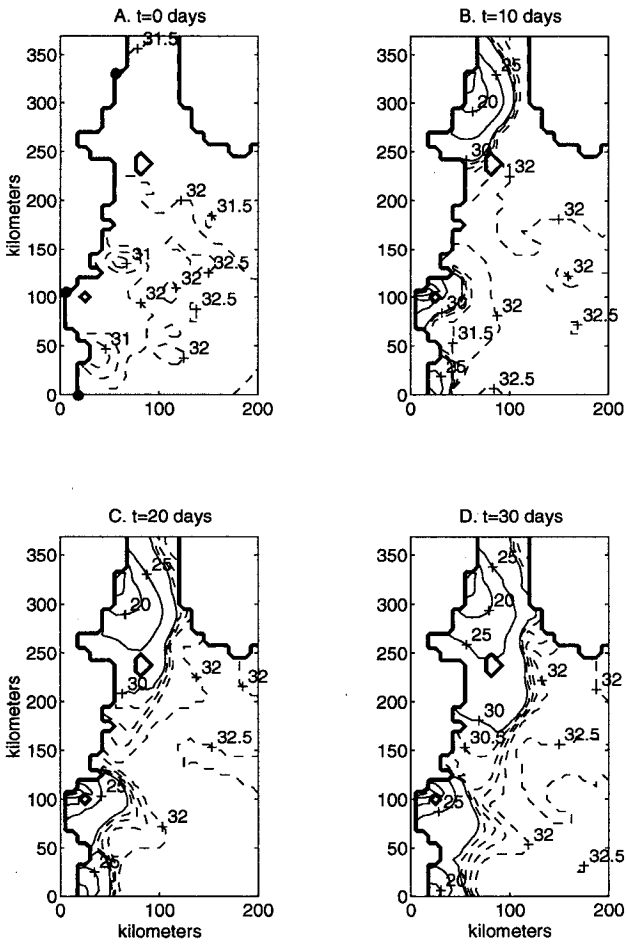

FIG. 14. Same as Fig. 13 except for surface salinity. Solid contours are shown with interval 5 ppt for salinities of 30 psu and less; the dashed contour interval is 0.5 ppt.

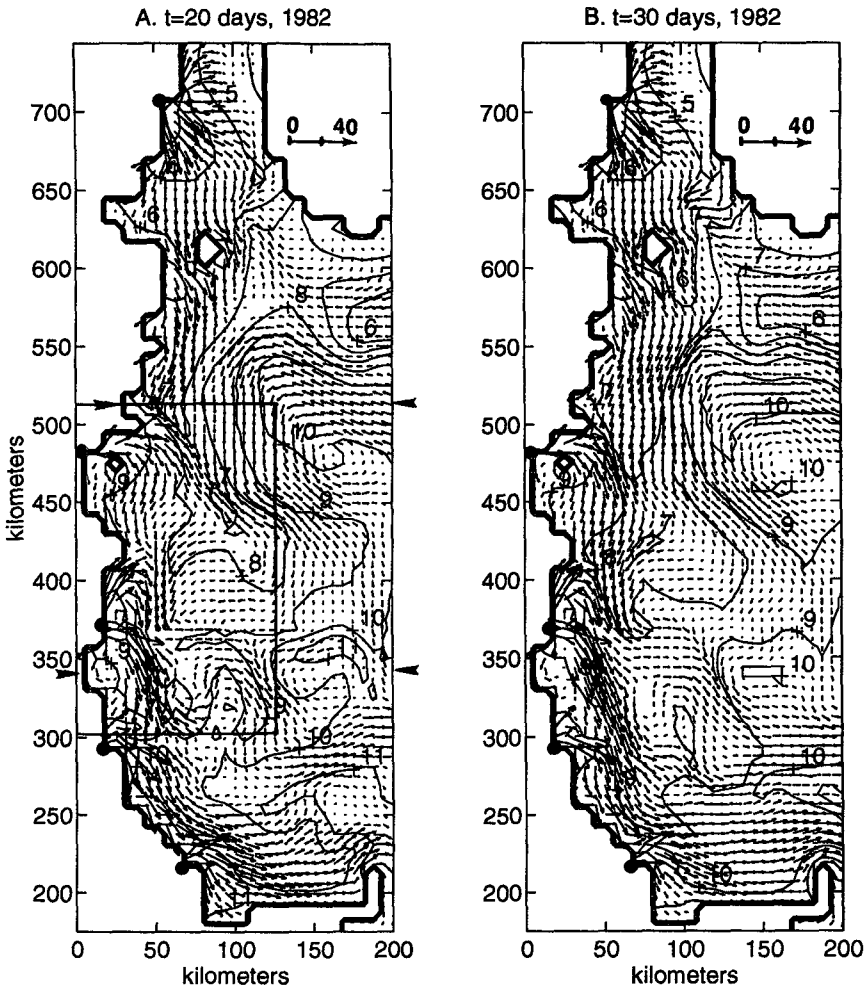

FIG. 15. Full-resolution residual surface currents and surface temperature (°C) for the coastal subdomain labeled C in Fig. 3, showing the development of the coastal current from the Bay of Fundy to Cape Cod at 20 and 30 days for the 1982 experiment. Fluxes from the principal rivers are given in Table 1, and the river mouths shown by the dots are identified on Fig. 1. Vector speed scale (cm s^{-1}) is indicated. Inset box refers to Fig. 17.

able data, even with the relatively fine spacing of the June 1982 hydrographic stations (Fig. 8 shows station locations). Inside the Bay of Fundy, where no stations were occupied on that cruise and initial values came from coarse-grid climatological averages, the initial surface temperature increases unrealistically toward the head of the bay, but by day 10 the strong tidal mixing in the bay has established the more typical cold surface temperatures found there and also along the tip of Nova Scotia.

Ten days after the model run begins, lowered surface salinity is apparent in the plumes from the Saint John, Penobscot, and Kennebec–Androscoggin Rivers (Fig. 14). All of the river plumes first bulge outward in both directions along the coast and then develop a coastal current that moves southwestward in the Kelvin wave sense, as in the first experiment with only the Saint John River. At 10 days, surface water fresher than 30 psu from the Saint John is just reaching Grand Manan Island. The relatively low surface temperatures advected in the developing coastal current form a tonguelike structure with an offshore minimum extending to Penobscot Bay; the 8°C isotherm shows that the offshore turn has begun east of the bay (Fig. 13). Subsequently, the river plumes continue to expand, and by 30 days surface water fresher than 30 psu is found 50 km southwest of Grand Manan Island. The outflow path from the Saint John favors the offshore side of the island, as shown by the 6°C surface isotherm, consistent with the earlier discussion about the development of the plume.

The full-resolution residual surface current and temperature for the coastal domain from the Bay of Fundy to Cape Cod (inset "C" in Fig. 3) are shown in

Fig. 15, for days 20 and 30 only. The surface salinity from the same region appears in Fig. 16, which compares the result at 30 days for the 1982 and 1983 cases. Figure 17 shows an expanded view of the surface currents and salinity in the region directly influenced by the Penobscot and Kennebec–Androscoggin Rivers (inset box in Figs. 15 and 16).

By 30 days in both years, surface waters with salinity <30 psu occupy a coastal strip 30–50 km wide that extends beyond the tip of Cape Cod (Fig. 16). In 1982 the eastern Maine coastal current, indicated by a prominent low-temperature surface tracer, separates from the coast where it encounters the eastern thermohaline front defining the Penobscot River plume and carries relatively cool and fresh water offshore (Fig. 15). Part of the deflected current joins an anticlockwise flow in Jordan Basin, while the remainder either continues offshore or returns shoreward to feed the coastal current that reforms west of Penobscot Bay. The temperature and salinity fronts on the eastern side of Penobscot Bay intensify and move slightly southwest as the coastal current intensifies, so that by day 30 the offshore deflection has partly "healed" and a larger fraction of the coastal current continues past the bay than at day 20. Farther to the west, a branch of the freshwater moves away from the coast where the coastal current encounters the outflow from the Kennebec–Androscoggin Rivers. The offshore flow brings relatively fresh and cool water toward Wilkinson Basin and eventually Georges Bank (Fig. 12). The remainder of the coastal current continues toward Cape Cod with comparatively little interruption by the Saco and Merrimack Rivers, which have smaller flow rates than the other rivers (Table 1).

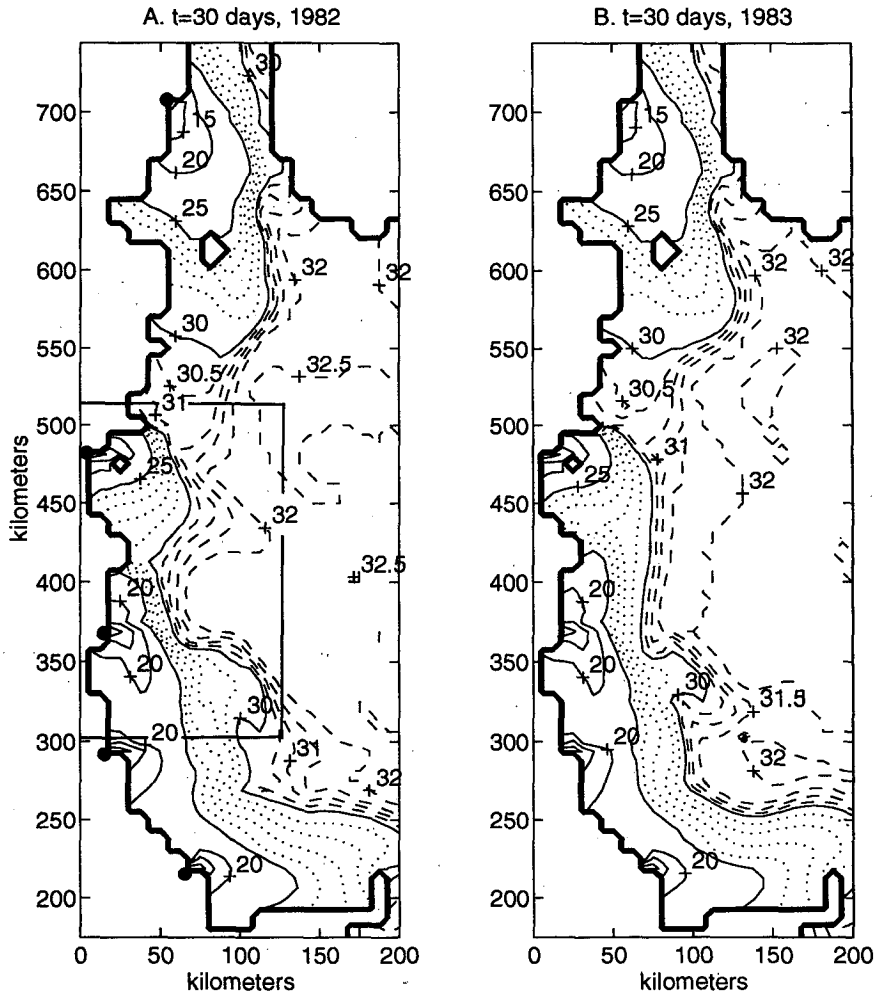

FIG. 16. Tidal-residual surface salinity (ppt) for the coastal domain C identified in Fig. 3, comparing result at t = 30 days for model experiments initialized with composite data from June 1982 (a) and June 1983 (b). River mouths are shown by the dots in (a). The contour interval is 5 ppt for salinity < 30 psu and 0.5 ppt for salinity > 30 psu. Dotted contours show detail between 25 and 30 psu with 1 ppt interval. Inset box refers to Fig. 17.

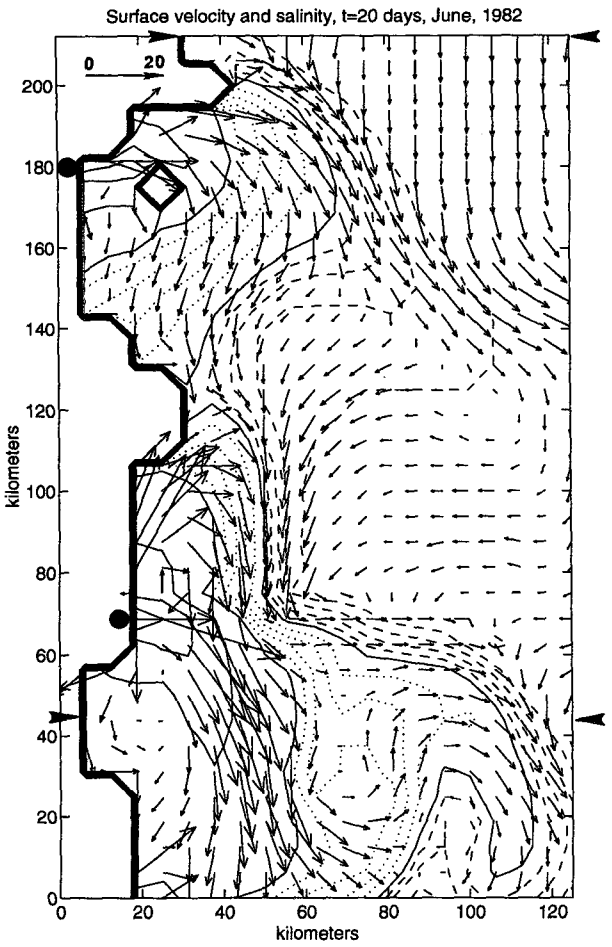

FIG. 17. Detail of the full-resolution residual surface current and salinity at $t = 20$ days for the 1982 case. The region of detail, which includes the mouths of the Penobscot and Kennebec–Androscoggin Rivers (dots), is shown by the inset box in Fig. 15. Salinity contours (unlabeled) are the same as those in Fig. 16. Vector speed scale (cm s^{-1}) is indicated. The horizontal arrowheads show locations of vertical sections in later figures.

In both 1982 and 1983 cases, the freshened Saint John River plume divides around Grand Manan Island as the water spreads along the coast (Fig. 16). The axis of lowest surface salinity persists in the offshore path, as noted in the first experiment with only the Saint John River and no external forcing. In both years, a strong salinity front from the Penobscot River forms at about the same location east of Penobscot Bay, but in 1983 there is a smaller salinity contrast with offshore water, which is about 0.5 ppt fresher after 30 days than in the 1982 case. The plume from the Kennebec–Androscoggin River also spreads in both directions along the coast, but its eastern surface salinity front, for convenience defined by the 25 and 30 psu isohalines, is somewhat weaker than the one east of Penobscot Bay; nevertheless, the coastal current is partially deflected offshore as it is guided around the plume boundary.

The expanded view of the midcoast region (Fig. 17) shows that at 20 days the coastal current is guided around the river plumes following a salinity front that is stronger on the upstream (eastern) side of the Penobscot and Kennebec–Androscoggin River mouths. The coastal current converges in the fronts, then diverges as part of the surface flow moves offshore and part returns toward shoreward to join the reformed coastal current downstream of the river outflow. After 20 days in the 1982 experiment, the thermohaline front in the Kennebec–Androscoggin plume has expanded eastward about 30 km from the river mouth and is beginning to merge with freshened water from the Penobscot River, located about 100 km to the east; by 30 days, as the plumes continue to merge, the 30 ppt salinity contour moves offshore from Penobscot Bay to Cape Cod (Fig. 16a). Eastward expansion of the plume from the Penobscot River appears to be limited by the headlands that form the eastern side of Penobscot Bay. Evidently the considerable eastward extension of the Kennebec–Androscoggin plume causes the coastal current to divide into two branches separated by complex eddying, whereas a more diffuse spreading of the coastal current is associated with the Penobscot plume.

Eastward movement of water from the Kennebec–Androscoggin River is clearly indicated by satellite images of suspended sediment during the spring flood of 1987 (Stumpf and Goldschmidt 1992), and long-term persistence of eastward flow from the major rivers is shown by grain size distributions in bottom sediments (Ross 1970). According to anecdotal reports from the early 1960s and before, when Maine rivers still provided the primary means of transporting wood to the paper industry, errant pulp logs from the Kennebec occasionally drifted into Linekin Bay, about 20 km to the east of the river mouth (L. Hartford 1993, personal communication). Evidence for an offshore moving branch of the coastal current in the southwestern gulf can be found in the surface salinity, which in the "wet" June of 1983 was <30 psu over the northern part of Wilkinson Basin about 100 km south of Casco Bay; at the same location the upper level current was southward in a 10-week mean (Fig. 2).

e. Vertical sections

We now examine the subsurface structure along vertical sections perpendicular to the coast at Blue Hill Bay and at Casco Bay, respectively located immediately upstream of the offshore deflection east of Penobscot Bay and immediately downstream of the Kennebec–Androscoggin plume. The section locations are indicated by the horizontal arrowheads in Figs. 15a and 17. At 20 days in the 1982 model experiment, the lowered temperature and salinity in the coastal current are evident on the Blue Hill section, with minima about 25 km offshore that extend to the bottom (Fig. 18).

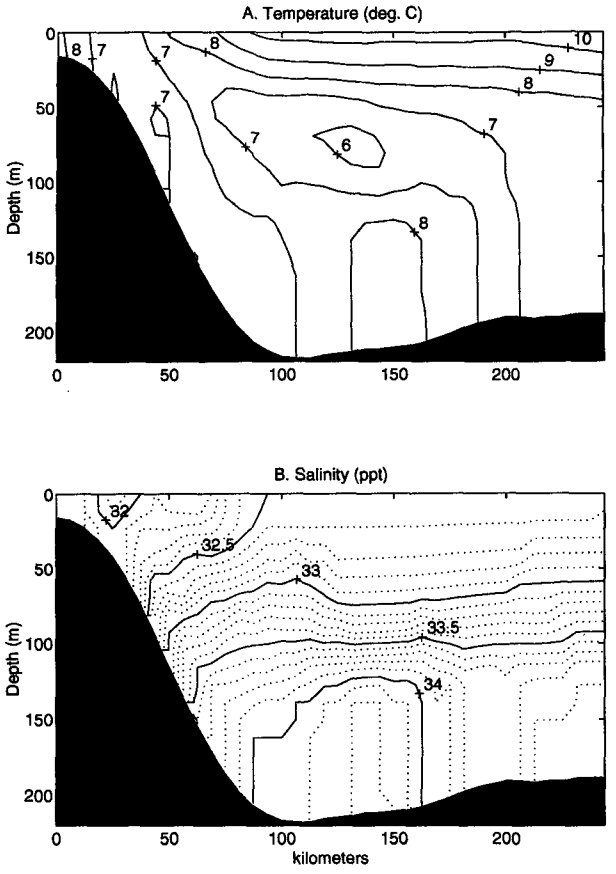

FIG. 18. Tidal-residual temperature [(a), °C] and salinity on a vertical section extending offshore from Blue Hill Bay (location shown by the horizontal arrowheads in Figs. 15 and 17). The contour intervals are 1°C and 0.1 ppt.

Farther offshore, a thin layer of relatively warm and saline surface water overlies Maine intermediate water (MIW), revealed by its characteristic temperature minimum <6°C near 75-m depth. Over the deepest part of the section, in the center of Jordan Basin, the relatively high salinity (>34 psu) and temperature (>8°C) indicates bottom water of Atlantic slope origin.

The longshore residual velocity across the Blue Hill section is shown in Fig. 19 together with the effective vertical eddy viscosity (A_V), also averaged over a tidal cycle. At 20 days, the coastal current has a double-core structure at this location. The inner, more intense core with surface speeds >12 cm s^{-1} extends nearly to the bottom; this flow turns offshore and follows the thermohaline front defining the outer boundary of the plume from the Penobscot River, as shown in plan view in Figs. 15a and 17. The broader and weaker outer core mostly bypasses the river plume and moves offshore toward Wilkinson Basin in the southwestern gulf, although a fraction, shown by the dashed contours, turns back to the northeast and contributes to a weak anticlockwise gyre in Jordan Basin. The magnitude of the near-bottom vertical eddy viscosity in the inner core of the coastal current (about 80×10^{-4} m^2 s^{-1}) indicates an Ekman-scale height in the bottom boundary layer of about 10 m, and this is resolved by 3 or 4 sigma levels at the local depth of about 30 m. Near the bottom of Jordan Basin, where the Richardson number is reduced by tidal shear, the eddy viscosity increases to about 10^{-1} m^2 s^{-1} and the corresponding boundary-layer scale thickness is about 40 m, spanned by 3 sigma levels at that depth. Thus, the boundary layer is represented in a rudimentary sense in the 10-level model formulation.

Later in the experiment, at 30 days, the MIW temperature minimum on the Blue Hill section is weakened and the nearshore surface salinity in the coastal current decreases to less than 31 psu as the influence of the Saint John River continues to spread along the coast (30-day sections are not shown). The increasing flow compresses the thermohaline front on the east side of the Penobscot plume, the offshore deflection decreases, and the double-core structure of the longshore flow collapses into a broader single-core flow that follows a more direct path around the plume to rejoin the flow along the coast southwest of Penobscot Bay (Fig. 15).

The coastal current is also interrupted by the Kennebec–Androscoggin plume, as noted earlier, and the lowered temperatures and salinities in the coastal current form a near-surface layer about 30 m thick that extends about 100 km offshore off Casco Bay at 20 days (Fig. 20). The considerable offshore spread of the freshened surface water near this section results from the outer branch of the separated coastal current, which flows almost directly offshore at the surface between 70 and 100 km on the Casco Bay section. The minimum surface salinity, indicating the axis of the inner branch of the coastal current where it crosses the section, is about 35 km offshore. The temperature minimum of the MIW core is obvious near 75-m depth over the inner part of Wilkinson Basin, and also farther offshore where the section approaches the inner edge of Georges Bank. The two temperature minima are separated by warmer and more saline bottom water of Atlantic origin that spreads into the deepest part of Wilkinson Basin along a direct pathway from Northeast Channel.

The longshore velocity across the section (Fig. 21) shows that the inner branch of the reformed coastal current off Casco Bay has a maximum surface speed of about 18 cm s^{-1} and extends essentially to the bottom, with a secondary maximum just above the bottom near the 60-m isobath. Associated with the near-bottom flow is a salinity maximum (Fig. 20), which traces the movement of bottom water along the coast from the inner edge of Jordan Basin in the eastern gulf. The eddy viscosity near the bottom under the coastal current indicates a boundary-layer thickness of about 7 m, which is resolved by two model levels at the 60-m

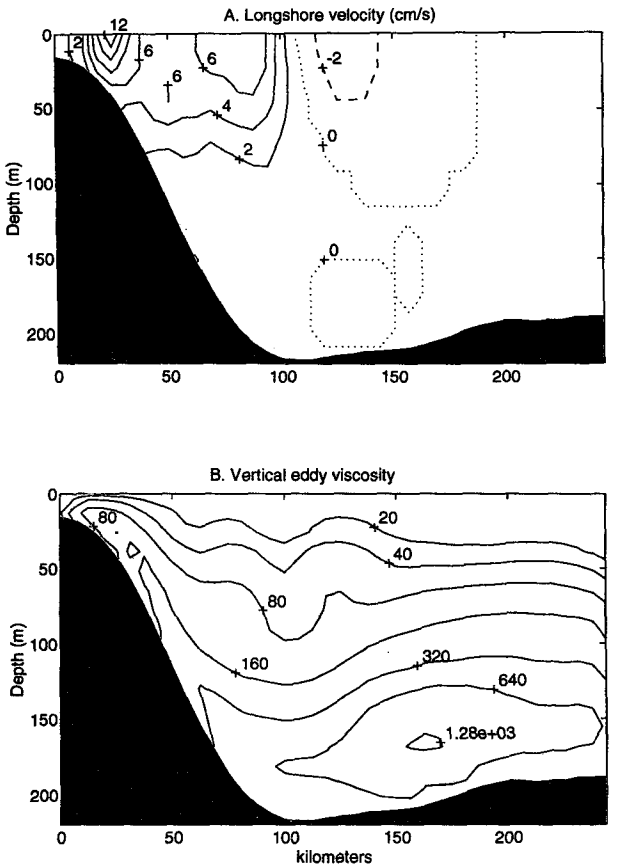

FIG. 19. Tidal-residual longshore velocity [(a), cm s^{-1}] and vertical eddy viscosity [(b), cm^2 s^{-1}] on the Blue Hill vertical section located by the arrowheads in Figs. 15 and 17. The velocity is contoured with interval 2 cm s^{-1}. Solid contours indicate southwestward flow along the Maine coast in the Kelvin wave sense; the zero contour is dotted. For the eddy viscosity, successive contours indicate doubling of the value.

isobath. The outer branch of the longshore flow, which has a maximum surface speed of about 6 cm s^{-1} and is confined to the upper half of the water column, crosses the section about 110 km offshore. The several reversals of the longshore velocity result from the sinuous path of the offshore branch as it meanders across the Casco Bay section toward Wilkinson Basin (Fig. 15).

A small part of the coastal current immediately adjacent to the coast enters the east side of Casco Bay, bringing a direct river influence into the surface waters of the bay (Fig. 21); the nearshore path is seen in plan view in Fig. 17. Pollutants from the Kennebec River are known to enter the bay by this pathway (Larsen 1992). A clockwise eddy forms seaward of the bay in the region where the coastal current re-forms west of the Kennebec–Androscoggin River mouth, also bringing river-influenced water toward Casco Bay, but from its southwest side (dashed contours nearest the shore in Fig. 21); the eddy circulation is mostly beneath the surface and therefore not evident in Fig. 17. The model experiment suggests that the flushing of Casco Bay may be more complicated than previously thought, with important influences from offshore and the south as well as directly from the Kennebec outflow to the east.

5. Summary

The long-term objective of the modeling effort for the Gulf of Maine is to develop an improved dynamical understanding of the seasonal baroclinic circulation in the gulf and near the offshore banks. Ultimately, this will lead to prognostic simulations of the 3D velocity field and the coupled density field, given adequate initial and boundary data. As a step in that direction, the present study focuses on the buoyancy-driven circulation in the inner basins and near the coast, where the influence of relatively fresh water from rivers and the Scotian shelf is important. The advection terms were excluded from the momentum equations but retained in the equations for temperature and salinity, which gives a quasi-linear prognostic scheme that includes

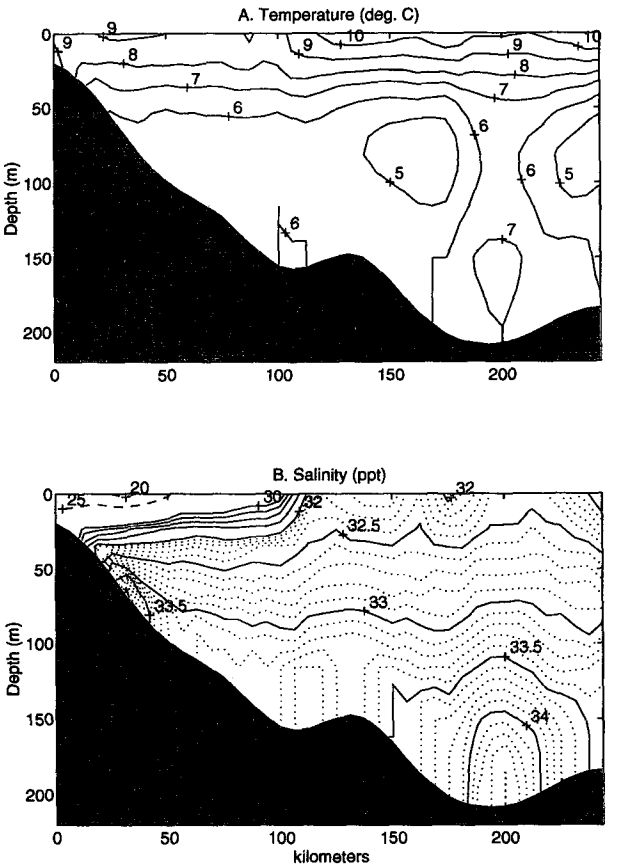

FIG. 20. Same as Fig. 18 except for a section offshore of Casco Bay, shown by the arrowheads on Figs. 15 and 17. The contour interval is 5 ppt for salinity < 30 psu (dashed) and 1 ppt for salinity between 30 and 32 psu.

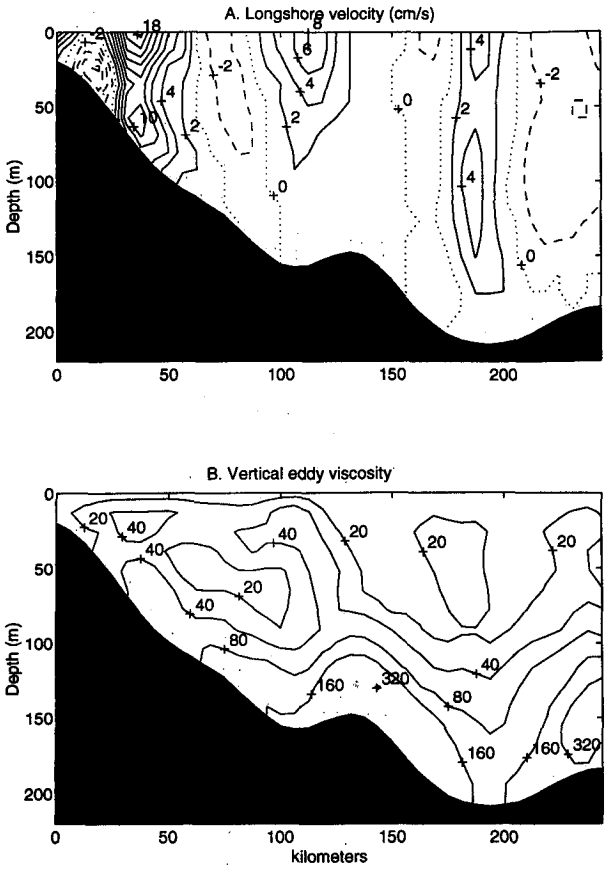

FIG. 21. Same as Fig. 19 except for the Casco Bay section, located by the arrowheads in Figs. 15 and 17.

self-advection of density but excludes tidal rectification and other nonlinear effects. The model experiments use composite datasets assembled from June hydrographic observations blended with climatological data to set initial and boundary conditions. External forcing is provided by the semidiurnal tide and by prescribed inflow from the Nova Scotian shelf; the important influences of wind and seasonal heating are not considered here.

A central result is that the principal rivers significantly impact the coastal circulation in the upstream direction, that is, in the sense opposite to the right-bounded development expected in the Northern Hemisphere. The model experiments show that each river outflow initially forms a bulge that expands in both directions along the coast. Thereafter a coastal plume escapes the bulge and spreads in the Kelvin wave sense, consistent with the findings by Chao and Boicourt (1986) that set the stage for the present work. For example, the plume from the Penobscot River expands several tens of kilometers to the east of Penobscot Bay, where a sharp thermohaline front partially deflects offshore the current flowing along the eastern Maine coast. Part of the redirected flow recirculates in Jordan Basin in the eastern gulf, another part contributes to a larger-scale anticlockwise gyre in the central gulf, and the remainder turns shoreward again to join a reformed coastal current west of Penobscot Bay. Thus, the Penobscot plume may play an important role in determining the extent to which tidally mixed, nutrient-rich water carried in the eastern Maine coastal current is directed toward the central gulf, where weaker tidal mixing allows surface warming, increased stratification, and enhanced biological production in the spring and summer months.

Farther to the west, the combined outflow from the Kennebec and Androscoggin Rivers has a similar influence, and again part of the coastal current is guided offshore in a thermohaline front that forms east of the river mouth. The deflected flow crosses Wilkinson Basin and mostly turns back to the northeast along the inner edge of Georges Bank as part of the large-scale anticlockwise circulation in the gulf. The coastal current re-forms off Casco Bay, southwest of the Kennebec–Androscoggin plume, and then continues on toward Cape Cod and the shelf beyond with comparatively little interruption by the smaller Saco and Merrimack Rivers. A back eddy off Casco Bay brings water toward the bay from the south, and this may be an underappreciated pathway for pollutants from the Kennebec River.

More complete models of the Gulf of Maine region will include fluxes of heat and moisture at the sea surface, in addition to forcing by the wind, tides, and shelf inflow. Together, these factors control the thermohaline transition between late winter when surface cooling and winds produce deep convection and mixing and early summer when the winds abate and the surface waters in the central and western gulf restratify as solar heating increases. A three-part working hypothesis for the vernal intensification of the circulation can be advanced to guide future model studies and field observations: 1) the accumulation and deep convection of fresh and cold water inside the gulf in late winter recharges the MIW and retards deep inflow through Northeast Channel by establishing an offshore pressure gradient; 2) the onset of surface stratification and upwelling-favorable winds in early summer weakens the deep pressure gradient and allows dense Atlantic slope water to enter the gulf and spread over sills into the interior basins; and 3) the accumulation of slope water, particularly in Georges and Jordan Basins, intensifies the upper-level circulation in the eastern basins and the interior gulf as a whole. According to this hypothesis, the intensity, structure, and timing of the interior circulation that develops each summer depends on a competition between freshwater sources and convection in the previous winter, which tend to delay the indraft of Atlantic slope water, and surface restratification and winds in the late spring, which encourage deep water inflow and intensification of the upper-level currents. The year-to-year variations in the observed

summer circulation suggest that small changes in one factor—for example, river runoff—can have a major influence on the development process. Numerical models offer a convenient way to explore such ideas by varying one factor while holding others fixed, a procedure not often possible with field experiments. It is primarily for this reason that model experiments, tempered by observations, offer the prospect of improved understanding of the circulation in the Gulf of Maine.

Acknowledgments. The numerical modeling studies reported here were supported by Grant OCE91-15554 from the National Science Foundation. Kurt Hess and his colleagues wrote the original model code known as MECCA and willingly made it available to me. Thor Aarup helped modify the code to accommodate large grid sizes. Ms. Link Ji worked with me to develop the composite initial datasets. Several of the figures were created with software called Ferret, which was kindly made available by Steve Hankin of NOAA's Pacific Marine Environmental Laboratory.

While developing an appreciation for the foibles and pitfalls of numerical models, I have frequently been reminded of the importance of "real" data as the ultimate reality check. I am pleased to acknowledge the many students, colleagues, and friends who helped gather the observations that eventually motivated this study. I also appreciate the helpful and detailed comments provided by several anonymous reviewers of an earlier version of this paper.

APPENDIX

Summary Description of the Numerical Model

a. Governing equations

A numerical model known as MECCA (Model for Estuarine and Coastal Circulation Assessment: Hess 1989) was used to solve the discretized equations governing conservation of momentum, mass, heat, and salt on a beta plane, subject to the hydrostatic and Boussinesq approximations (Gill 1982). In an orthogonal Cartesian coordinate system with horizontal coordinates (x, y) and vertical coordinate z increasing upward from the sea surface, the linearized equations expressing conservation of momentum are, in the x direction:

$$\frac{\partial u}{\partial t} - fv = -\frac{1}{\rho_0}\frac{\partial p}{\partial x} + \frac{\partial}{\partial z}\left(A_v \frac{\partial u}{\partial z}\right) + F_u, \quad (1)$$

in the y direction:

$$\frac{\partial v}{\partial t} + fu = -\frac{1}{\rho_0}\frac{\partial p}{\partial y} + \frac{\partial}{\partial z}\left(A_v \frac{\partial v}{\partial z}\right) + F_v, \quad (2)$$

and in the vertical the hydrostatic balance:

$$\rho g = -\frac{\partial p}{\partial z}. \quad (3)$$

The conservation equation for temperature (T) is

$$\frac{\partial T}{\partial t} + \mathbf{v}\cdot\nabla T = \frac{\partial}{\partial z}\left(D_v \frac{\partial T}{\partial z}\right) + D_T + R \quad (4)$$

where R represents sources/sinks of temperature, and a similar equation holds for the conservation of salt (S). The fluid density ρ is determined by a general equation of state

$$\rho = \rho_0[1 + F_\rho(S, T)]$$

in which F_ρ is an empirical function used to calculate the perturbation density from the temperature and salinity (Mamaev 1964). Finally, conservation of mass is expressed by the continuity equation

$$\frac{\partial u}{\partial x} + \frac{\partial v}{\partial y} + \frac{\partial w}{\partial z} = 0. \quad (5)$$

In (1)–(5), (u, v, w) are the components of a 3D velocity vector $\mathbf{v}$ with (x, y, z) components in the (east, north, upward) directions. The Coriolis parameter $f = 2\omega \sin\theta$, where ω is the angular rotation rate of the earth and θ is the latitude. Latitudinal variation of the Coriolis parameter is introduced by means of the beta-plane approximation, $f = f_0 + \beta y$, where f_0 is the value of f at reference latitude θ_0, $\beta = df/dy$, and the origin of the coordinate system is defined so that $y = 0$ at the reference latitude.

For the Gulf of Maine application, the nonlinear advection terms were dropped from the momentum equations (1) and (2) to avoid nonphysical oscillations in cases with strong tidal currents (speeds exceeding about 1 m s^{-1}). The instability apparently arises from the first-order upwind discretization used for the advection terms, a problem that may be alleviated in future applications by using a higher-order differencing scheme (Fletcher 1988). However, the advection terms were retained without difficulty in the equation for temperature (4) and in the corresponding equation for salinity, which results in a quasi-linear prognostic scheme useful for studying the development of buoyancy-driven flows.

b. Mixing and diffusion

In (1)–(4), F_u, F_v, $D_{T,S}$ are terms representing turbulent horizontal mixing and diffusion (Blumberg and Mellor 1987):

$$F_u = \frac{\partial}{\partial x}\left[2A_h \frac{\partial u}{\partial x}\right] + \frac{\partial}{\partial y}\left[A_h\left(\frac{\partial u}{\partial y} + \frac{\partial v}{\partial x}\right)\right]$$

$$F_v = \frac{\partial}{\partial y}\left[2A_h \frac{\partial v}{\partial y}\right] + \frac{\partial}{\partial x}\left[A_h\left(\frac{\partial u}{\partial y} + \frac{\partial v}{\partial x}\right)\right]$$

$$D_{T,S} = \frac{\partial}{\partial x} D_h \frac{\partial(T, S)}{\partial x} + \frac{\partial}{\partial y} D_h \frac{\partial(T, S)}{\partial y}. \quad (6)$$

The eddy momentum terms F_u, F_v are approximations to the full stress tensor with the scaling simplification that the vertical divergence can be neglected in (5) (Mellor and Blumberg 1985). With this assumption, the eddy momentum flux reduces to the more usual Laplacian form in the case A_h = const.

The instantaneous vertical turbulent viscosity and diffusion coefficients (A_v and D_v) in (1)–(4) are calculated using a modified Munk–Anderson (1948) formula based on a mixing length, the local vertical shear of the horizontal velocity, and the local stratification:

$$A_V = A_{V00} + \frac{A_Z}{(1 + 10\ \mathrm{Ri})^{1/2}} + A_{V0}$$

$$D_V = D_{V00} + \frac{A_Z}{(1 + 3.3\ \mathrm{Ri})^{3/2}} + D_{V0},$$

where

$$A_z = \left[\kappa z\left(1 + \frac{z}{H}\right)\right]^2\left[\left(\frac{\partial u}{\partial z}\right)^2 + \left(\frac{\partial v}{\partial z}\right)^2\right]^{1/2}$$

is the mixing length–dependent coefficient for neutral stratification (Ri = 0), and the Richardson number Ri is given by

$$\mathrm{Ri} = -\frac{g}{\rho_0}\frac{\partial \rho}{\partial z}\left[\left(\frac{\partial u}{\partial z}\right)^2 + \left(\frac{\partial v}{\partial z}\right)^2\right]^{-1}.$$

In this formulation, A_{V00} and D_{V00} are initializing values set at 25×10^{-4} m^2 s^{-1} and 10×10^{-4} m^2 s^{-1}, respectively; A_{V0} and D_{V0} are background values of 10^{-5} m^2 s^{-1}; and κ is the von Kármán constant (0.4). The initial values are updated in the model at each internal time step as $A_V^n = (A_V^{n-1}A_V)^{1/2}$, where superscript n indicates the current time step; D_V is updated similarly. The mixing length scale increases from zero at the surface and bottom to a maximum at middepth, where $z = -H/2$. The Munk–Anderson constants in the above formulas are typical values used in continental shelf and slope applications (e.g., Hamilton and Rattray 1978; Foo et al. 1981; Endoh et al. 1981). During model experiments, instantaneous vertical mixing ("convection") is implemented in the event of unstable vertical density gradients.

The horizontal turbulent viscosity in the model depends on the local velocity shear and deformation and the grid spacing ΔL according to the Smagorinsky (1963) formula,

$$A_h = A_{h0} + C_3\Delta L^2\left[2\left(\frac{\partial u}{\partial x}\right)^2 + 2\left(\frac{\partial v}{\partial y}\right)^2 + \left(\frac{\partial u}{\partial y} + \frac{\partial v}{\partial x}\right)^2\right]^{1/2},$$

where C_3 is a constant with a value of 10^{-2} and A_{h0} is a small background horizontal viscosity of 10 m^2 s^{-1}. As noted by Mellor and Blumberg (1985), in the absence of motion the Smagorinsky formulation essentially removes cross-slope eddy diffusion along sigma surfaces, which would otherwise (e.g., in the case of A_h constant) produce a baroclinically driven flow starting from no motion.

c. Boundary conditions

In the present study there is no wind stress, so the surface boundary condition is $\tau_{sx,sy} = (0, 0)$. The stress in the x direction at the ocean bottom is parameterized by

$$\tau_{bx} = \rho C_d u_b(u_b + v_b)^{1/2}$$

and similarly in the y direction, where u_b and v_b are components of the near-bottom current vector. The dimensionless quadratic drag coefficient C_d was set at 6.4×10^{-3}, somewhat larger than the more typical 2.5×10^{-3} commonly used in vertically averaged models (e.g., Davies 1993) but the same as that chosen by Greenberg (1977) in a model of the upper Bay of Fundy and similar to the value used by Loder and Wright (1985) to parameterize the bottom stress over the inner flank of Georges Bank. Recently, Sucsy et al. (1993) used tidal current data to "tune" a 3D tidal model for the full Gulf of Maine region, finding that the best choice for the quadratic bottom drag coefficient was 6×10^{-3}. In the present study, numerous experiments were run with drag coefficients in the range 2×10^{-3} to 8×10^{-3} to investigate the sensitivity of the model to bottom drag. The tidal-residual results shown here do not depend substantially on the exact value chosen. The larger value may be appropriate because the prominent tidal currents amplify the effective tidally averaged bottom stress (Rooth 1972).

At the ocean boundaries, a time-dependent water elevation or tide height is specified at the center of each grid cell defining the boundary. An interpolation procedure or an initializing dataset is used to provide initial values of temperature and salinity at all levels in all grid cells. Freshwater fluxes from rivers are included by augmenting the water level in the cell at the river mouth at the rate $Q_R/(\Delta L^2)$, where Q_R is the river flux and ΔL is the horizontal cell spacing. The rate of salinity change in the cell containing the river is

$$\frac{\partial}{\partial t}(HS) = 0,$$

and the rate of change of temperature T in the cell is given by

$$\frac{\partial(HT)}{\partial t} = T_R Q_R/\Delta L^2,$$

where H is the total water depth in the cell and T_R is the river temperature.

On the cross-shelf and along-shelf open boundaries, an Orlanski-style radiation condition is used to mini-

mize wave reflections, following Chapman (1985). The Orlanski approach uses the local long-wave gravity wave speed to set the advection of model variables across open boundaries. In cases with variable depth and stratification, this leads to some distortion of the fields near the edges of the model domain, since disturbances traveling with different phase speeds are imperfectly transmitted through the open boundaries. Absorptive "sponge" layers with greatly increased friction adjacent to the open boundaries can be used to reduce inward reflections but at the cost of additional subjectivity in model parameter choices. Preliminary experiments in the present study indicate that sponge layers provide somewhat smoother fields near open boundaries but the differences were small and did not significantly affect the interior circulation that forms the basis of this work.

d. *Vertical coordinate*

A terrain-following, or sigma, vertical coordinate is used to transform (1)–(6) so that the physical space between a variable bottom depth and a free sea surface is stretched into a fixed domain convenient for numerical calculations (Phillips 1957). The details of the transformation are given by Blumberg and Mellor (1987), for example, and are not repeated here. The sigma transform is useful in applications to complex coastal or continental shelf regions but at the expense of additional terms in the transformed equations and grid-dependent truncation errors in the pressure gradient terms (Haney 1991). Mellor and Blumberg (1985) point out that the sigma transform projects a component of turbulent mixing along sigma surfaces into the vertical direction, so that over steep bottom slopes the bottom boundary layer may be misrepresented in typical applications where A_h is much larger than A_v. To minimize these problems, practical applications of sigma-coordinate numerical models generally require some combination of smoothed bottom topography and fine horizontal and vertical grid resolution.

e. *Implementation*

The MECCA code (Hess 1989) solves the vertically averaged momentum equations to obtain the external-mode velocity and sea level height, using an alternating-direction implicit (ADI) scheme (Fletcher 1988). The residual momentum equations are solved for the internal mode, using an implicit scheme to determine the horizontal velocity components at each level in each grid cell. The vertical velocity at each level is then determined diagnostically from the continuity equation. A staggered placement of variables within the grid cell is used, with the horizontal velocity components specified on the orthogonal sides of the cell and the sea level height and vertical velocity specified at the cell center, corresponding to a C grid. The mode-splitting technique allows the internal mode to be calculated on a time step longer than that used for the free surface deformation and the vertically integrated velocities.

The ADI scheme is known to be unconditionally stable when applied to the inviscid Burgers equation (which excludes pressure gradient and Coriolis accelerations), with a truncation error of order Δt^2, where Δt is the time step (Fletcher 1988). When horizontal viscosity is included there is a limitation on the time step set by eddy diffusion, but the diffusional limitation is generally much less restrictive than the Courant–Fredrich–Levy (CFL) stability condition, which limits the external-mode time step in an explicit formulation to $\Delta t_e < \Delta L/(gH_{\max})^{1/2}$; here Δt_e is the maximum allowable time step for the external mode, ΔL is the horizontal grid cell spacing, and $H_{\max}$ is the maximum depth in the model domain. For the internal mode, the time-step limitation in an equivalent explicit scheme is $\Delta t_i < \Delta z^2/4\,A_v$, where Δz is the local vertical interval between sigma levels and A_V is the vertical eddy viscosity. This limitation would be prohibitively restrictive in the present application, for which the explicit limit is Δt_i of order 1 s, but with the implicit vertical scheme the CFL limitation has proven to be adequately restrictive and was adopted for the quasi-linear prognostic model experiments. For the Gulf of Maine examples shown here, the external time step was $\Delta t_e = 62.1$ s, chosen to satisfy the CFL condition and also to synchronize the M_2 tidal period of 12.42 hours, which allows calculation of the tidal-residual fields by averaging over an exact tidal cycle. The internal-mode time step used for all cases reported here was $\Delta t_i = 5\Delta t_e$.

REFERENCES

Apollonio, S., 1979: *The Gulf of Maine.* Courier-Gazette Books, 60 pp.

Bigelow, H. B., 1927: Physical oceanography of the Gulf of Maine. *Fish. Bull.*, **40**, 511–1027.

Blumberg, A. F., and G. L. Mellor, 1987: A description of a three-dimensional coastal ocean circulation model. *Three-Dimensional Coastal Ocean Models,* N. Heaps, Ed., Amer. Geophys. Union, 208 pp.

Brooks, D. A., 1985: Vernal circulation in the Gulf of Maine. *J. Geophys. Res.*, **90**(C5), 4687–4705.

——, 1987: Currents at Lindenkohl Sill in the southern Gulf of Maine. *J. Geophys. Res.*, **95**(C12), 22 173–22 192.

——, 1993: A brief overview of the physical oceanography of the Gulf of Maine. *Proc. of the Gulf of Maine Scientific Workshop,* Woods Hole, MA, Urban Harbors Institute, University of Massachusetts, 404 pp.

——, and E. S. Gottlieb, 1985: Springtime hydrographic surveys in the Gulf of Maine: 1982, 1983, and 1984. Tech. Rep. No. 85-3-T, Texas A&M University, 234 pp.

——, and D. W. Townsend, 1989: Variability of the coastal current and nutrient pathways in the Gulf of Maine. *J. Mar. Res.*, **47**, 303–321.

Brown, W. S., 1984: A comparison of Georges Bank, Gulf of Maine and New England Shelf tidal dynamics. *J. Phys. Oceanogr.*, **14**, 145–167.

——, and R. C. Beardsley, 1978: Winter circulation in the western Gulf of Maine: Part 1. Cooling and water mass formation. *J. Phys. Oceanogr.*, **8**, 265–277.

——, and J. D. Irish, 1992: The annual evolution of geostrophic flow in the Gulf of Maine. *J. Phys. Oceanogr.*, **22**, 445–473.

Bumpus, D. F., 1960: Sources of water contributed to the Bay of Fundy by surface circulation. *J. Fish. Res. Bd. Can.*, **17**(2), 181–197.

——, and L. M. Lauzier, 1965: Surface circulation on the continental shelf of eastern North America between Newfoundland and Florida. *Ser. Atlas of the Marine Environment*, Folio 7, Am. Geogr. Soc.

Butman, B., R. C. Beardsley, B. Magnell, D. Frye, J. A. Vermersch, R. Schlitz, R. Limburner, W. R. Wright, and M. A. Noble, 1982: Recent observations of the mean circulation on Georges Bank. *J. Phys. Oceanogr.*, **12**, 569–591.

Chao, S-Y., and W. C. Boicourt, 1986: Onset of estuarine plumes. *J. Phys. Oceanogr.*, **16**, 2137–2149.

Chapman, D. C., 1985: Numerical treatment of cross-shelf open boundaries in a barotropic coastal ocean model. *J. Phys. Oceanogr.*, **15**, 1060–1075.

——, and R. C. Beardsley, 1989: On the origin of shelf water in the Middle Atlantic Bight. *J. Phys. Oceanogr.*, **19**(3), 384–391.

Davies, A. M., 1993: A bottom boundary layer-resolving three-dimensional tidal model: A sensitivity study of eddy viscosity formulation. *J. Phys. Oceanogr.*, **23**, 1437–1453.

Drinkwater, K., B. Petrie, and W. H. Sutcliffe Jr., 1979: Seasonal geostrophic transports along the Scotian shelf. *Estuar. Coastal Mar. Sci.*, **9**, 17–27.

Endoh, M., C. N. K. Mooers, and W. R. Johnson, 1981: A coastal upwelling circulation model with eddy viscosity depending on Richardson number. *Coastal Upwelling*, F. A. Richards, Ed., Amer. Geophys. Union, 203–208.

Fletcher, C. A. J., 1988: *Computational Techniques for Fluid Dynamics*. Vol. 1. Springer-Verlag, 409 pp.

Foo, E.-C., C. Rooth, and R. Bleck, 1981: A two-dimensional diabatic isopycnal model of a coastal upwelling front. *Coastal Upwelling*. Coastal and Estuarine Sciences, No. 1, F. A. Richards, Ed., Amer. Geophys. Union, 193–202.

Garrett, C., 1972: Tidal resonance in the Bay of Fundy and Gulf of Maine. *Nature*, **238**, 441–443.

Gill, A. E., 1982: *Atmosphere–Ocean Dynamics*. Academic Press, 662 pp.

Graham, J. J., 1970: Coastal currents of the western Gulf of Maine. *Int. Comm. Northwest Atlantic Fish. Res. Bull.*, **7**, 19–31.

Greenberg, D. A., 1977: Mathematical studies of tidal behaviour in the Bay of Fundy. Manuscript Report Series, No. 46, Marine Sciences Directorate, Ottawa, 127 pp.

——, 1979: A numerical model investigation of tidal phenomena in the Bay of Fundy and Gulf of Maine. *Mar. Geodyn.*, **2**, 161–187.

——, 1983: Modeling the mean barotropic circulation in the Bay of Fundy and Gulf of Maine. *J. Phys. Oceanogr.*, **13**(5), 886–904.

——, 1990: The contribution of modeling to understanding the dynamics of the Bay of Fundy and Gulf of Maine. *Modeling Marine Systems*, A. M. Davies, Ed., CRC Press, 107–140.

Hamilton, P., and M. Rattray Jr., 1978: A numerical model of the depth-dependent, wind-driven upwelling circulation on a continental shelf. *J. Phys. Oceanogr.*, **8**, 437–457.

Haney, R. L., 1991: On the pressure gradient force over steep topography in sigma coordinate ocean models. *J. Phys. Oceanogr.*, **21**, 610–619.

Hess, K. W., 1989: MECCA program documentation. NOAA Tech. Rep. NESDIS 46, Washington, DC, 258 pp.

Hopkins, T. S., and N. Garfield, 1979: Gulf of Maine Intermediate Water. *J. Mar. Res.*, **37**, 103–139.

Isaji, T., and M. L. Spaulding, 1984: A model of the tidally induced residual circulation in the Gulf of Maine and Georges Bank. *J. Phys. Oceanogr.*, **14**, 1119–1126.

——, ——, and M. Reed, 1984: *A Numerical Modeling Characterization of the Annual Three-Dimensional Circulation in the Georges Bank–Gulf of Maine Region*. Appl. Sci. Assoc. Inc., 64 pp.

Johnson, D. F., and K. W. Hess, 1990: Numerical simulations of blue crab larval dispersal and recruitment. *Bull. Mar. Sci.*, **46**(1), 195–213.

Larsen, P. F., 1992: Marine environmental quality in the Gulf of Maine: A review. *Rev. Aquatic Sci.*, **6**, 67–87.

Limeburner, R., and R. C. Beardsley, 1982: The seasonal hydrography and circulation over Nantucket Shoals. *J. Mar. Res.*, **40**(Suppl.), 371–406.

Loder, J. W., 1980: Topographic rectification of tidal currents on the sides of Georges Bank. *J. Phys. Oceanogr.*, **10**, 1399–1416.

——, and D. G. Wright, 1985: Tidal rectification and frontal circulation on the sides of Georges Bank. *J. Mar. Res.*, **43**, 581–604.

——, and D. A. Greenberg, 1986: Predicted positions of tidal fronts in the Gulf of Maine region. *Contin. Shelf. Res.*, **6**(3), 397–414.

Lynch, D. R., F. E. Werner, D. A. Greenberg, and J. W. Loder, 1992: Diagnostic model for baroclinic, wind-driven and tidal circulation in shallow seas. *Contin. Shelf Res.*, **12**, 37–64.

Mamaev, O. I., 1964: A simplified relationship between density, temperature and salinity of sea water. *Akad. Nauk., Geophys. Sers.*, **2**, 180–181.

Mellor, G. L., and A. F. Blumberg, 1985: Modeling vertical and horizontal diffusivities with the sigma coordinate system. *Mon. Wea. Rev.*, **113**, 1379–1383.

Munk, W. H., and E. R. Anderson, 1948: Notes on the theory of the thermocline. *J. Mar. Res.*, **7**, 276–295.

Phillips, O. M., 1957: A coordinate system having some special advantages for numerical forecasting. *J. Meteor.*, **14**, 184–185.

Ramp, S. R., R. J. Schlitz, and W. R. Wright, 1985: The deep flow through the Northeast Channel, Gulf of Maine. *J. Phys. Oceanogr.*, **15**, 1790–1808.

Rooth, C., 1972: A linearized bottom friction law for large-scale oceanic motions. *J. Phys. Oceanogr.*, **2**, 509–510.

Ross, D. A., 1970: Atlantic continental shelf and slope of the United States—Heavy minerals of the continental margin from southern Nova Scotia to northern New Jersey. U.S. Geological Survey Prof. Paper 529-G, 40 pp.

Smagorinsky, J., 1963: General circulation experiments with the primitive equations I: The basic experiment. *Mon. Wea. Rev.*, **91**, 99–164.

Smith, P. C., 1983: The mean and seasonal circulation off southwest Nova Scotia. *J. Phys. Oceanogr.*, **13**, 1034–1054.

——, 1989: Seasonal and interannual variability of current, temperature and salinity off southwest Nova Scotia. *Can. J. Fish. Aquatic Sci.*, **46**, 4–20.

Stumpf, R. P., and P. M. Goldschmidt, 1992: Remote sensing of suspended sediment discharge into the western Gulf of Maine during the April 1987 100-year flood. *J. Coastal Res.*, **8**(1), 218–225.

Sucsy, P. V., B. R. Pearce, and V. G. Panchang, 1993: Comparison of two- and three-dimensional model simulation of the effect of a tidal barrier on the Gulf of Maine tides. *J. Phys. Oceanogr.*, **23**, 1231–1248.

Vermersch, J. A., and R. C. Beardsley, 1979: Winter circulation in the western Gulf of Maine: Part 2. Current and pressure observations. *J. Phys. Oceanogr.*, **9**, 768–784.

Weatherly, G. L., and P. J. Martin, 1978: On the structure and dynamics of the oceanic bottom boundary layer. *J. Phys. Oceanogr.*, **8**, 557–570.

Wright, D. G., D. A. Greenberg, J. W. Loder, and P. C. Smith, 1986: The steady-state barotropic response of the Gulf of Maine and adjacent regions to surface wind stress. *J. Phys. Oceanogr.*, **16**, 947–966.